Commun. Comput. Phys.
doi: 10.4208/cicp.021114.140715a

Vol. **19**, No. 2, pp. 442-472
February 2016

An Adaptive Finite Element Method with Hybrid Basis for Singularly Perturbed Nonlinear Eigenvalue Problems

Ye Li*

Department of Mathematical Sciences, Tsinghua University, Beijing 100084, China.

Received 2 November 2014; Accepted (in revised version) 14 July 2015

Abstract. In this paper, we propose an uniformly convergent adaptive finite element method with hybrid basis (AFEM-HB) for the discretization of singularly perturbed nonlinear eigenvalue problems under constraints with applications in Bose-Einstein condensation (BEC) and quantum chemistry. We begin with the time-independent Gross-Pitaevskii equation and show how to reformulate it into a singularly perturbed nonlinear eigenvalue problem under a constraint. Matched asymptotic approximations for the problem are reviewed to confirm the asymptotic behaviors of the solutions in the boundary/interior layer regions. By using the normalized gradient flow, we propose an adaptive finite element with hybrid basis to solve the singularly perturbed nonlinear eigenvalue problem. Our basis functions and the mesh are chosen adaptively to the small parameter ε. Extensive numerical results are reported to show the uniform convergence property of our method. We also apply the AFEM-HB to compute the ground and excited states of BEC with box/harmonic/optical lattice potential in the semiclassical regime ($0<\varepsilon\ll 1$). In addition, we give a detailed error analysis of our AFEM-HB to a simpler singularly perturbed two point boundary value problem, show that our method has a minimum uniform convergence order $\mathcal{O}(1/(N\ln N)^{\frac{2}{3}})$.

AMS subject classifications: 35P30, 35Q55, 65N25, 65N06, 65N30, 81Q05

Key words: Adaptive finite element, hybrid basis, nonlinear eigenvalue problem, singularly perturbed problem, Bose-Einstein condensation, uniform convergence.

1 Introduction

We consider the following nonlinear eigenvalue problem which is known as the time independent Gross-Pitaevskii equation (GPE) in Bose-Einstein condensation (BEC) [2, 4,

*Corresponding author. *Email address:* yeli11@mails.tsinghua.edu.cn (Y. Li)

 ©2016 Global-Science Press

https://doi.org/10.4208/cicp.021114.140715a Published online by Cambridge University Press

9, 14]:

$$\mu\phi(\mathbf{x}) = -\frac{1}{2}\Delta\phi(\mathbf{x}) + V(\mathbf{x})\phi(\mathbf{x}) + \beta|\phi(\mathbf{x})|^2\phi(\mathbf{x}), \qquad \mathbf{x}\in\Omega, \tag{1.1}$$

$$\phi(\mathbf{x}) = 0, \qquad \mathbf{x}\in\partial\Omega, \tag{1.2}$$

where $\mathbf{x} = (x_1,\cdots,x_d)^T$ is the spatial coordinate, Ω is a subdomain of $\mathbb{R}^d$ ($d = 1,2,3$), $V(\mathbf{x})$ is a real-valued potential, and β is a constant. The wave function ϕ is required to satisfy the normalization condition

$$\|\phi\|^2 = \int_\Omega |\phi(\mathbf{x})|^2 d\mathbf{x} = 1. \tag{1.3}$$

The eigenvalue (chemical potential) μ is computed by

$$\mu(\phi) = \int_\Omega \left(\frac{1}{2}|\nabla\phi(\mathbf{x})|^2 + V(\mathbf{x})|\phi(\mathbf{x})|^2 + \beta|\phi(\mathbf{x})|^4\right) d\mathbf{x}. \tag{1.4}$$

The energy is computed by

$$E(\phi) = \int_\Omega \left(\frac{1}{2}|\nabla\phi(\mathbf{x})|^2 + V(\mathbf{x})|\phi(\mathbf{x})|^2 + \frac{\beta}{2}|\phi(\mathbf{x})|^4\right) d\mathbf{x}. \tag{1.5}$$

In fact, the nonlinear eigenvalue problem (1.1)-(1.2) can be viewed as the Euler-Lagrange equation of the energy functional $E(\phi)$ under the normalization constraint (1.3). In physical literatures [3, 11, 37], the ground state $\phi_g(\mathbf{x})$ and k-th excited state $\phi_k(\mathbf{x})$ are defined as the local minimizer of the energy functional over the unit sphere

$$S = \{\phi \,|\, \|\phi\| = 1,\ \ E(\phi) < \infty\}, \tag{1.6}$$

which are ranked according to their energies, i.e.,

$$E(\phi_g) < E(\phi_1) < E(\phi_2) < \cdots. \tag{1.7}$$

One of the fundamental problems in numerical simulation of BEC is to find its ground and excited states so as to compare the numerical results with experimental observations and to prepare initial data for studying the dynamics of BEC. Different numerical methods were proposed for computing the ground and excited states of BEC. For example, Bao and Du [9] presented a continuous normalized gradient flow with diminishing energy for computing the ground and first excited states in BEC. This idea was extended to multi-component BEC [4,10], rotating BEC [16], spin-1 BEC [7,12,15] and dipolar BEC [6]. Bao and Tang [14] proposed a method by directly minimizing the energy functional via finite element approximation to obtain the ground and excited states. Zhou [45, 46] and Shen and Zhou [42] provided error estimates for the finite element approximations for some nonlinear eigenvalue problems. In recent years, Zhou et al. [17, 24, 41] also used the adaptive finite element method to compute some eigenvalue problems arising in

https://doi.org/10.4208/cicp.021114.140715a Published online by Cambridge University Press

quantum physics and incompressible flows. Chang et al. [20] proposed Gauss-Seidel-type methods for computing energy states of a multi-component BEC. Edwards and Burnett [26] presented a Runge-Kutta type method and used it to solve one and three dimensional ground states with spherical symmetry. Adhikari [1] used this approach to get the ground state solution of GPE in 2D with radial symmetry. Other approaches include an explicit imaginary-time algorithm used by Cerimele et al. [19] and Chiofalo et al. [22], a direct inversion in the iterated subspace (DIIS) used by Schneider et al. [40], and a simple analytical type method proposed by Dodd [25]. For more information about the mathematical and numerical theory of BEC we refer the reader to the review paper [5] by Bao and Cai.

We mainly consider the case $\beta \gg 1$, i.e. in strongly repulsive interaction regime. As observed in [8, 13], boundary/interior layers will appear when $\beta \to \infty$. In this case, all the above numerical methods which in general use uniform meshes do not converge uniformly with respect to $\beta \gg 1$. In fact, we can do a semiclassical re-scaling to transform the problem into a singularly perturbed problem. After we use the normalized gradient flow method combined with the semi-implicit backward Euler discretization in time, we only need to solve a singularly perturbed reaction-diffusion equation (3.6) in each iteration. Some special techniques are needed to treat the singular perturbation problem. We can use Shishkin mesh (also known as piecewise uniform mesh, layer-adapted mesh [35, 36, 44]) if we know the positions and widths of boundary/interior layers. Bao and Chai [8] combine the normalized gradient flow and Shishkin mesh technique to get an uniformly convergent result for the singularly perturbed nonlinear eigenvalue problem. Some special schemes can also be robust on uniform mesh. For example, Han and Huang [27, 28] proposed the tailored finite point method (TFPM) for steady state singularly perturbed convection-diffusion-reaction equation, their method can achieve high accuracy even on coarse mesh. TFPM is also uniformly convergent for some cases [29, 31], but the uniformly convergent error analysis is still open for the general case. Chin and Krasny [21] proposed a hybrid asymptotic finite element method for stiff two-point boundary value problem. Stynes an O'Riordan [38, 43] proposed exponentially fitted finite element method for a singular perturbed two-point boundary value problem, and their method was complemented by Jiang and Yue [32]. Both of these methods used the exact solutions of local approximated problems as the basis functions. Lin and Stynes [33] proposed a balanced finite element method for the singularly perturbed linear reaction-diffusion problem, where a balanced norm (stronger than the standard energy norm) was introduced and uniform convergence was proved on a Shishkin mesh. Melenk et al. [34] also used so-called *hp*-version finite element method to achieve uniform convergence. For more related work about robust numerical methods for singularly perturbed differential equations, please refer to the book by Roos, Stynes and Tobiska [39].

In this paper we propose an adaptive finite element method with hybrid basis for the singularly perturbed nonlinear eigenvalue problem (1.1)-(1.2). Based on the asymptotic solutions, we choose our basis functions and the mesh adaptively to the small parameter ε, so our method can be uniformly convergent for all $\varepsilon > 0$. The paper is organized as fol-

https://doi.org/10.4208/cicp.021114.140715a Published online by Cambridge University Press

lows. In Section 2 we reformulate the time-independent GPE into a singularly perturbed nonlinear eigenvalue problem with box and harmonic potential, respectively. Matched asymptotic approximations are also reviewed to give the asymptotic solutions in 1D as well as in higher dimensions. In Section 3 we propose the adaptive finite element method with hybrid basis for the singularly perturbed nonlinear eigenvalue problem. In Section 4 we give numerous numerical examples to demonstrate the efficiency of our method and to compare with other existing numerical methods. In the appendix we give a detailed error analysis of our method to a singularly perturbed two point boundary value problem, and prove our method to be uniformly convergent.

2 A singularly perturbed nonlinear eigenvalue problem

In this section, we reformulate the time-independent GPE (1.1) into a singularly perturbed nonlinear eigenvalue problem under a constraint when $\beta \gg 1$, i.e., in strongly repulsive interaction regime. We also review the matched asymptotic approximations for the ground state and excited states as well as their energy and chemical potential of the corresponding singularly perturbed nonlinear eigenvalue problem. We will list the asymptotic results here, and the details can be found in [8, 13].

2.1 For bounded Ω with box potential

When Ω is bounded and $V(\mathbf{x})$ is chosen as a box potential, i.e. $V(\mathbf{x})\equiv 0$ in Ω and $V(\mathbf{x})=\infty$ outside, let

$$\varepsilon := \frac{1}{\sqrt{\beta}}, \quad \mu^\varepsilon := \frac{\mu}{\beta}, \quad \phi^\varepsilon(\mathbf{x}) := \phi(\mathbf{x}), \tag{2.1}$$

then the time-independent GPE problem (1.1)-(1.3) is reformulated to the following singularly perturbed nonlinear eigenvalue problem

$$\mu^\varepsilon \phi^\varepsilon(\mathbf{x}) = -\frac{\varepsilon^2}{2}\Delta\phi^\varepsilon(\mathbf{x}) + |\phi^\varepsilon(\mathbf{x})|^2\phi^\varepsilon(\mathbf{x}), \qquad \mathbf{x}\in\Omega, \tag{2.2}$$

$$\phi^\varepsilon(\mathbf{x}) = 0, \qquad \mathbf{x}\in\partial\Omega, \tag{2.3}$$

with a normalization constraint

$$\|\phi^\varepsilon\|^2 = \int_\Omega |\phi^\varepsilon(\mathbf{x})|^2 d\mathbf{x} = 1. \tag{2.4}$$

The re-scaled eigenvalue (chemical potential) μ^ε is computed by

$$\mu^\varepsilon := \mu^\varepsilon(\phi^\varepsilon) = \int_\Omega \left(\frac{\varepsilon^2}{2}|\nabla\phi^\varepsilon(\mathbf{x})|^2 + |\phi^\varepsilon(\mathbf{x})|^4\right) d\mathbf{x} = \mathcal{O}(1), \tag{2.5}$$

and the re-scaled energy is computed by

$$E^\varepsilon := E^\varepsilon(\phi^\varepsilon) = \int_\Omega \left(\frac{\varepsilon^2}{2}|\nabla\phi^\varepsilon(\mathbf{x})|^2 + \frac{1}{2}|\phi^\varepsilon(\mathbf{x})|^4\right) d\mathbf{x} = \mathcal{O}(1). \tag{2.6}$$

https://doi.org/10.4208/cicp.021114.140715a Published online by Cambridge University Press

Now we review the asymptotic results of the singularly perturbed nonlinear eigenvalue problem (2.2)-(2.4). For simplicity, we first consider $\Omega=[0,1]$. By matched asymptotic expansion, we get the approximation for the ground state when $0<\varepsilon\ll 1$:

$$\phi_g^\varepsilon(x)\approx\phi_g^{MA}(x)=\sqrt{\mu_g^{MA}}\Big[\tanh\Big(\sqrt{\mu_g^{MA}}x/\varepsilon\Big)+\tanh\Big(\sqrt{\mu_g^{MA}}(1-x)/\varepsilon\Big)-\tanh\Big(\sqrt{\mu_g^{MA}}/\varepsilon\Big)\Big],\qquad 0\le x\le 1. \tag{2.7}$$

Plugging it into the normalization constraint (2.4), after some computations, we obtain

$$1=\int_0^1|\phi_g^\varepsilon(x)|^2dx\approx\mu_g^{MA}-2\varepsilon\sqrt{\mu_g^{MA}}. \tag{2.8}$$

Solving it we obtain the asymptotic approximation for the chemical potential of the ground state as

$$\mu_g^\varepsilon\approx\mu_g^{MA}\approx 1+2\varepsilon\sqrt{1+\varepsilon^2}+2\varepsilon^2. \tag{2.9}$$

Moreover, we can obtain the asymptotic approximation for the energy of the ground state as

$$E_g^\varepsilon\approx E_g^{MA}\approx\frac{1}{2}+\frac{4}{3}\varepsilon\sqrt{1+\varepsilon^2}+2\varepsilon^2. \tag{2.10}$$

Similarly, we get the asymptotic solution for the k-th excited state as

$$\phi_k^\varepsilon(x)\approx\sqrt{\mu_k^{MA}}\left[\sum_{j=0}^{[(k+1)/2]}\tanh\left(\frac{\sqrt{\mu_k^{MA}}}{\varepsilon}\left(x-\frac{2j}{k+1}\right)\right)+\sum_{j=0}^{[k/2]}\tanh\left(\frac{\sqrt{\mu_k^{MA}}}{\varepsilon}\left(\frac{2j+1}{k+1}-x\right)\right)-C_k\tanh\left(\frac{\sqrt{\mu_k^{MA}}}{\varepsilon}\right)\right], \tag{2.11}$$

where $[t]$ takes the integer part of the real number t, the constant $C_k=1$ when k is even and $C_k=0$ when k is odd. The asymptotic approximations of eigenvalue and energy of the k-th excited state are given by

$$\mu_k^\varepsilon\approx\mu_k^{MA}\approx 1+2(k+1)\varepsilon\sqrt{1+(k+1)^2\varepsilon^2}+2(k+1)^2\varepsilon^2, \tag{2.12}$$

$$E_k^\varepsilon\approx E_k^{MA}\approx\frac{1}{2}+\frac{4}{3}(k+1)\varepsilon\sqrt{1+(k+1)^2\varepsilon^2}+2(k+1)^2\varepsilon^2. \tag{2.13}$$

Similar to 1D case, we can extend the matched asymptotic approximations for the 1D ground state and k-th excited states to higher dimensions, i.e. d-dimensions ($d=2,3$). In the region $\Omega=[0,1]^d$, the matched asymptotic approximations for the ground state and

https://doi.org/10.4208/cicp.021114.140715a Published online by Cambridge University Press

$\mathbf{k}=(k_1,\cdots,k_d)$-th excited state in d-dimensions with $\mathbf{x}=(x_1,\cdots,x_d)$ are

$$\phi_{\mathbf{k}}^{\varepsilon}(x)\approx\sqrt{\mu_{\mathbf{k}}^{MA}}\prod_{i=1}^{d}\left[\sum_{j=0}^{[(k_i+1)/2]}\tanh\left(\frac{\sqrt{\mu_{\mathbf{k}}^{MA}}}{\varepsilon}\left(x_i-\frac{2j}{k_i+1}\right)\right)\right.$$
$$\left.+\sum_{j=0}^{[k_i/2]}\tanh\left(\frac{\sqrt{\mu_{\mathbf{k}}^{MA}}}{\varepsilon}\left(\frac{2j+1}{k_i+1}-x_i\right)\right)-C_{k_i}\tanh\left(\frac{\sqrt{\mu_{\mathbf{k}}^{MA}}}{\varepsilon}\right)\right], \quad (2.14)$$

And the asymptotic approximations of chemical potential and energy functional can be computed by the normalization constraint (2.4) and the above expression (2.14). Especially when $k:=k_1=k_2=\cdots=k_d$ we have the following expressions:

$$\mu_{\mathbf{k}}^{\varepsilon}\approx\mu_{\mathbf{k}}^{MA}\approx 1+2d(k+1)\varepsilon\sqrt{1+d(2-d)(k+1)^2\varepsilon^2}+2d(k+1)^2\varepsilon^2, \quad (2.15)$$
$$E_{\mathbf{k}}^{\varepsilon}\approx E_{\mathbf{k}}^{MA}\approx\frac{1}{2}+\frac{4d}{3}(k+1)\varepsilon\sqrt{1+d(2-d)(k+1)^2\varepsilon^2}+\frac{1}{3}d(d+5)(k+1)^2\varepsilon^2. \quad (2.16)$$

From the above asymptotic results, we can draw the following conclusions:

- Boundary layers are observed at $x=0$ and $x=1$ for the ground and all excited states when $0<\varepsilon\ll 1$, and for k-th excited state there are k interior layers located at $x_j=\frac{j}{k+1}, j=1,2,\cdots,k$. The width of these layers are $\mathcal{O}(\varepsilon)=\mathcal{O}(\beta^{-1/2})$.
- When $0<\varepsilon\ll 1$, if all the eigenfunctions are ranked according to their energies, then the corresponding eigenvalues (or chemical potentials) are ranked in the same order. This suggests that the two definitions of the ground state used in physical literatures: (1) minimizer of energy functional, (2) eigenfunction of the nonlinear eigenvalue problem with smallest eigenvalue, are equivalent.

These information will be used in designing our adaptive finite element method with hybrid basis for the singularly perturbed nonlinear eigenvalue problem (2.2)-(2.4).

2.2 For the whole space $\Omega=\mathbb{R}^d$ with harmonic potential

When $\Omega=\mathbb{R}^d$ is the whole space and $V(\mathbf{x})$ is chosen as the harmonic potential, i.e.

$$V(\mathbf{x})=\frac{1}{2}(\gamma_1^2x_1^2+\cdots+\gamma_d^2x_d^2), \quad (2.17)$$

with $\gamma_1,\cdots,\gamma_d$ positive constants (for simplicity we assume $\gamma_1=\cdots=\gamma_d=1$ below), we choose the semiclassical re-scaling as

$$\varepsilon:=\beta^{-\frac{2}{d+2}}, \quad \tilde{\mathbf{x}}:=\varepsilon^{\frac{1}{2}}\mathbf{x} \quad \mu^{\varepsilon}:=\varepsilon\mu, \quad \phi^{\varepsilon}(\tilde{\mathbf{x}}):=\varepsilon^{-\frac{d}{4}}\phi(\mathbf{x}). \quad (2.18)$$

https://doi.org/10.4208/cicp.021114.140715a Published online by Cambridge University Press

Substituting the above re-scaling parameters into the time-independent GPE (1.1), dropping the symbol ˜, we again obtain the following singularly perturbed nonlinear eigenvalue problem

$$\mu^{\varepsilon}\phi^{\varepsilon}(\mathbf{x}) = -\frac{\varepsilon^2}{2}\Delta\phi^{\varepsilon}(\mathbf{x}) + V(\mathbf{x})\phi^{\varepsilon}(\mathbf{x}) + |\phi^{\varepsilon}(\mathbf{x})|^2\phi^{\varepsilon}(\mathbf{x}), \qquad \mathbf{x}\in\mathbb{R}^d, \tag{2.19}$$

with a normalization constraint

$$\|\phi^{\varepsilon}\|^2 = \int_{\mathbb{R}^d} |\phi^{\varepsilon}(\mathbf{x})|^2 d\mathbf{x} = 1. \tag{2.20}$$

Again, the re-scaled eigenvalue (chemical potential) μ^{ε} is computed by

$$\mu^{\varepsilon} := \mu^{\varepsilon}(\phi^{\varepsilon}) = \int_{\mathbb{R}^d} \left(\frac{\varepsilon^2}{2}|\nabla\phi^{\varepsilon}(\mathbf{x})|^2 + V(\mathbf{x})|\phi^{\varepsilon}(\mathbf{x})|^2 + |\phi^{\varepsilon}(\mathbf{x})|^4 \right) d\mathbf{x} = \mathcal{O}(1), \tag{2.21}$$

and the re-scaled energy is computed by

$$E^{\varepsilon} := E^{\varepsilon}(\phi^{\varepsilon}) = \int_{\mathbb{R}^d} \left(\frac{\varepsilon^2}{2}|\nabla\phi^{\varepsilon}(\mathbf{x})|^2 + V(\mathbf{x})|\phi^{\varepsilon}(\mathbf{x})|^2 + \frac{1}{2}|\phi^{\varepsilon}(\mathbf{x})|^4 \right) d\mathbf{x} = \mathcal{O}(1). \tag{2.22}$$

Now we review the asymptotic results of the singularly perturbed nonlinear eigenvalue problem (2.19)-(2.20). Again for simplicity, we first present results for 1D case. By using the matched asymptotic expansion technique, we obtain the asymptotic approximation for the first excited state:

$$\begin{aligned} \phi_1^{\varepsilon}(x) &\approx \phi_1^{MA}(x) \\ &= \begin{cases} \sqrt{\mu_1^{MA}}\tanh\left(\frac{\sqrt{\mu_1^{MA}}x}{\varepsilon}\right) + \sqrt{\mu_1^{MA} - \frac{x^2}{2}} - \sqrt{\mu_1^{MA}}, & 0 < x \le \sqrt{2\mu_1^{MA}}, \\ \sqrt{\mu_1^{MA}}\tanh\left(\frac{\sqrt{\mu_1^{MA}}x}{\varepsilon}\right) - \sqrt{\mu_1^{MA} - \frac{x^2}{2}} + \sqrt{\mu_1^{MA}}, & -\sqrt{2\mu_1^{MA}} \le x \le 0, \\ 0, & \text{otherwise.} \end{cases} \end{aligned} \tag{2.23}$$

And the asymptotic approximations for the chemical potential and energy are given by

$$\mu_1^{\varepsilon} \approx \mu_1^{MA} = \frac{1}{2}\left(\frac{3}{2}\right)^{\frac{2}{3}} + \frac{\sqrt{2}}{2}\varepsilon + \mathcal{O}(\varepsilon^2), \tag{2.24}$$

$$E_1^{\varepsilon} \approx E_1^{MA} = \frac{3}{10}\left(\frac{3}{2}\right)^{\frac{2}{3}} + \frac{\sqrt{2}}{2}\varepsilon + \mathcal{O}(\varepsilon^2). \tag{2.25}$$

For higher dimensional results, i.e. $d-$dimensions ($d=2,3$), we can get the Thomas-Fermi approximation for the ground state as

$$\phi_g^{TF}(\mathbf{x}) = \begin{cases} \sqrt{\mu_g^{TF} - V(\mathbf{x})}, & V(\mathbf{x}) < \mu_g^{TF}, \\ 0, & \text{otherwise,} \end{cases} \tag{2.26}$$

https://doi.org/10.4208/cicp.021114.140715a Published online by Cambridge University Press

and the Thomas-Fermi approximations for the chemical potential and energy are

$$d=2: \qquad \mu_g^{TF}=\left(\frac{1}{\pi}\right)^{\frac{1}{2}}, \quad E_g^{TF}=\frac{2}{3}\left(\frac{1}{\pi}\right)^{\frac{1}{2}}, \tag{2.27}$$

$$d=3: \qquad \mu_g^{TF}=\frac{1}{2}\left(\frac{15}{4\pi}\right)^{\frac{2}{5}}, \quad E_g^{TF}=\frac{5}{14}\left(\frac{15}{4\pi}\right)^{\frac{2}{5}}. \tag{2.28}$$

We can also get the matched asymptotic approximation for the first excited state. For example, for the first $(1,0)$-th excited state in 2D, the asymptotic solution is

$$\begin{aligned}&\phi^{\varepsilon}_{(1,0)}(x_1,x_2)\approx\phi^{MA}_{(1,0)}(x_1,x_2)\\ &=\begin{cases}\sqrt{\mu-\frac{x_2^2}{2}}\left(\tanh(\frac{\sqrt{\mu}x_1}{\varepsilon})-1\right)+\sqrt{\mu-\frac{x_1^2+x_2^2}{2}}, & x_1>0 \text{ and } x_1^2+x_2^2<2\mu,\\ \sqrt{\mu-\frac{x_2^2}{2}}\left(\tanh(\frac{\sqrt{\mu}x_1}{\varepsilon})+1\right)-\sqrt{\mu-\frac{x_1^2+x_2^2}{2}}, & x_1<0 \text{ and } x_1^2+x_2^2<2\mu,\\ 0, & \text{otherwise.}\end{cases}\end{aligned} \tag{2.29}$$

And the asymptotic approximations for the chemical potential and energy are given by

$$\mu^{\varepsilon}_{(1,0)}\approx\mu=\left(\frac{1}{\pi}\right)^{\frac{1}{2}}+\frac{4\sqrt{2}}{3\pi}\varepsilon+\mathcal{O}(\varepsilon^2), \tag{2.30}$$

$$E^{\varepsilon}_{(1,0)}\approx E=\frac{2}{3}\left(\frac{1}{\pi}\right)^{\frac{1}{2}}+\frac{64\sqrt{2}}{45\pi}\varepsilon+\mathcal{O}(\varepsilon^2). \tag{2.31}$$

From the above asymptotic results, we can draw the following conclusions:

- For the ground state, there is no boundary and interior layers.
- For the first excited state, an interior layer is located at $x=0$ and the width is $\mathcal{O}(\varepsilon)=\mathcal{O}(\beta^{-\frac{2}{d+2}})$.

Again, these information will be used in designing the uniformly convergent adaptive finite element method with hybrid basis for the singularly perturbed nonlinear eigenvalue problem (2.19)-(2.20).

We also note that the asymptotic solution is continuous on the whole $\mathbb{R}$ but the first derivative is not continuous at $x=\pm\sqrt{2\mu_1}$. This is a typical behavior for solutions of free boundary value problems, which indicates that an interface layer correction has to be constructed in order to improve the approximation quality. In practical computations, we can reduce it to a bounded computational domain Ω (for example $\Omega=[-c,c]$) by setting $\phi|_{\partial\Omega}=0$.

https://doi.org/10.4208/cicp.021114.140715a Published online by Cambridge University Press

3 A uniformly convergent numerical method

3.1 The normalized gradient flow

The normalized gradient flow method, also known as 'imaginary time method' in physical literatures [2,4,9], has been widely used in the numerical computation for the ground state solution of BEC. It is one of the most popular and efficient techniques for dealing with the normalization constraint (2.20). The normalized gradient flow is a combination of steepest decent method and projection method:

$$\partial_t \phi(\mathbf{x},t) = \frac{\varepsilon^2}{2}\Delta\phi - V(\mathbf{x})\phi - |\phi|^2\phi, \quad \mathbf{x}\in\Omega,\ t_n < t < t_{n+1}, \tag{3.1}$$

$$\phi(\mathbf{x},t_{n+1}) = \phi(\mathbf{x},t_{n+1}^+) = \frac{\phi(\mathbf{x},t_{n+1}^-)}{\|\phi(\mathbf{x},t_{n+1}^-)\|}, \quad \mathbf{x}\in\Omega, \tag{3.2}$$

$$\phi(\mathbf{x},t) = 0, \quad x\in\partial\Omega, \qquad \phi(\mathbf{x},0) = \phi_0(\mathbf{x}), \quad \mathbf{x}\in\Omega; \tag{3.3}$$

where

$$\phi(\mathbf{x},t_n^\pm) = \lim_{t\to t_n^\pm}\phi(\mathbf{x},t), \qquad \|\phi_0\|^2 = \int_\Omega |\phi_0(\mathbf{x})|^2 d\mathbf{x} = 1.$$

Here and after we will omit the superscript ε for simplicity.

In one dimensional case, we choose the initial value $\phi(x,0) = \sqrt{2}\sin(\pi x)$ to compute the ground state of BEC with box potential, and $\phi(x,0) = \sqrt{2}\sin((k+1)\pi x)$ to compute the kth excited state of BEC with box potential, and $\phi(x,0) = \sin(\pi x/2)/\sqrt{2}$ to compute the first excited state of BEC with harmonic potential.

3.2 Discretization

In the following computation we use the semi-implicit backward Euler (BE) discretization in time:

$$\frac{\phi^* - \phi^n}{\tau} = \frac{\varepsilon^2}{2}\Delta\phi^* - V(x)\phi^* - |\phi^n|^2\phi^*, \tag{3.4}$$

$$\phi^{n+1}(x) = \frac{\phi^*(x)}{\|\phi^*(x)\|}, \tag{3.5}$$

and now we introduce an adaptive finite element with hybrid basis discretization in space.

First, we denote a general finite element framework discretization in space. For simplicity of notation we only consider the 1D case with $\Omega = (a,b)$. Generalization to higher dimensions are standard in references about finite element method [18]. Let $a = x_0 < x_1 < \cdots < x_N = b$ be a partition of the interval $\Omega = (a,b)$. The basis functions $\psi_i(x)$ $(i = 1,\cdots,N-1)$ are piecewise smooth and they satisfy $\psi_i(x_j) = \delta_{ij}$ for $j = 0,1,\cdots,N$. The finite dimensional space Φ_h is spanned by all $\psi_i(x)$ $(i = 1,\cdots,N-1)$.

https://doi.org/10.4208/cicp.021114.140715a Published online by Cambridge University Press

We rewrite the Eq. (3.4) as a reaction-diffusion equation

$$-\frac{\tau\varepsilon^2}{2}\Delta\phi^*(x)+(1+\tau V(x)+\tau|\phi^n(x)|^2)\phi^*(x)=\phi^n(x). \tag{3.6}$$

The corresponding variational problem is to find $\phi^*\in H_0^1(\Omega)$ such that

$$a(\phi^*,v)+c(\phi^*,v)=\langle\phi^n,v\rangle, \qquad \forall v\in H_0^1(\Omega), \tag{3.7}$$

and the corresponding finite element approximation problem is to find $\phi_h^*=\sum_{i=1}^{N-1}\phi_i^*\psi_i(x)$ such that

$$a(\phi_h^*,v_h)+c(\phi_h^*,v_h)=\langle\phi^n,v_h\rangle, \qquad \forall v_h\in\Phi_h, \tag{3.8}$$

where

$$a(\phi_h^*,v_h)=\sum_{i=0}^{N-1}\frac{\tau\varepsilon^2}{2}\int_{x_i}^{x_{i+1}}\nabla\phi_h^*\nabla v_h dx, \tag{3.9}$$

$$c(\phi_h^*,v_h)=\sum_{i=0}^{N-1}\int_{x_i}^{x_{i+1}}(1+\tau V(x)+\tau|\phi^n|^2)\phi_h^*(x)v_h(x)dx. \tag{3.10}$$

The normalization step is discretized as

$$\phi_i^{n+1}=\frac{\phi_i^*}{\|\phi_h^*\|}, \quad i=0,\cdots,N, \tag{3.11}$$

with

$$\|\phi_h^*\|=\sqrt{\sum_{i=0}^{N-1}\int_{x_i}^{x_{i+1}}|\phi_h^*(x)|^2dx}. \tag{3.12}$$

After stationary state is reached, we can compute the chemical potential and energy functional as follows

$$\mu:=\frac{\varepsilon^2}{2}\sum_{i=0}^{N-1}\int_{x_i}^{x_{i+1}}|\nabla\phi_h(x)|^2dx+\sum_{i=0}^{N-1}\int_{x_i}^{x_{i+1}}(V(x)|\phi_h(x)|^2+|\phi_h(x)|^4)dx, \tag{3.13}$$

$$E:=\frac{\varepsilon^2}{2}\sum_{i=0}^{N-1}\int_{x_i}^{x_{i+1}}|\nabla\phi_h(x)|^2dx+\sum_{i=0}^{N-1}\int_{x_i}^{x_{i+1}}(V(x)|\phi_h(x)|^2+\frac{1}{2}|\phi_h(x)|^4)dx. \tag{3.14}$$

So our goal is to construct a proper finite dimensional space Φ_h with a suitable mesh partition.

https://doi.org/10.4208/cicp.021114.140715a Published online by Cambridge University Press

3.3 Adaptive finite element with hybrid basis

Now we come to design an uniformly convergent finite element method for the BE gradient flow. The main feature of our method is that the choice of the basis functions and the mesh depend on the parameter ε. Generally, if ε is not small, the classical finite difference/element method on uniform mesh can work enough well; and if ε is small, then the basis functions will choose to be asymptotic solutions in boundary/interior layer regions and polynomial functions in smooth regions, respectively. So there will be a balance between the choice of the basis functions and the mesh and ε. We call it "Adaptive Finite Element Method with Hybrid Basis (AFEM-HB for short)". A detailed error analysis of our method applied to a simpler singularly perturbed two point boundary value problem has been given in the appendix.

For computing the ground state of BEC with box potential, let $0=x_0<x_1<\cdots<x_N=1$ be a partition of the interval $[0,1]$, we set

$$x_j = x_{j-1} + \begin{cases} h_1, & j=1, \\ h_2, & 2\le j\le N-1, \\ h_1, & j=N, \end{cases} \tag{3.15}$$

in which the two kinds of mesh sizes are

$$h_1 = \begin{cases} \sigma, & \varepsilon\le\gamma, \\ \frac{1}{N}, & \varepsilon>\gamma, \end{cases} \qquad h_2 = \frac{1-2h_1}{N-2}. \tag{3.16}$$

Here we call $\sigma=\min\{\frac{1}{4},\varepsilon\ln N\}$ the x-transition point and $\gamma=\gamma(N)=(\ln N)^{\frac{1}{3}}/N^{\frac{2}{3}}$ the ε-transition point. The x-transition point is chosen as that in Shishkin mesh, and the ε-transition point is chosen to obtain the maximum uniform convergence rate (see details in the appendix). We note that we take only one point in every boundary layer regions, and this mesh size is $\ln N$ times greater than ε.

Now we come to construct the hybrid finite element space Φ_h. Let $\{\psi_i\}_{i=2}^{N-1}$ be the standard piecewise linear hat functions that satisfy $\psi_i(x_j)=\delta_{ij}$ for $j=0,1,\cdots,N$. Let the other two hybrid basis functions ψ_1 and ψ_{N-1} be

$$\psi_1(x) = \begin{cases} \frac{\tanh(\frac{x}{\varepsilon})}{\tanh(\frac{h_1}{\varepsilon})}, & x\in[x_0,x_1), \\ \frac{x_2-x}{x_2-x_1}, & x\in[x_1,x_2), \\ 0, & \text{otherwise}, \end{cases} \tag{3.17}$$

$$\psi_{N-1}(x) = \begin{cases} \frac{\tanh(\frac{1-x}{\varepsilon})}{\tanh(\frac{h_1}{\varepsilon})}, & x\in(x_{N-1},x_N], \\ \frac{x-x_{N-2}}{x_{N-1}-x_{N-2}}, & x\in(x_{N-2},x_{N-1}], \\ 0, & \text{otherwise}. \end{cases} \tag{3.18}$$

https://doi.org/10.4208/cicp.021114.140715a Published online by Cambridge University Press

The hybrid finite element space is

$$\Phi_h := \text{span}\{\psi_1,\psi_2,\cdots,\psi_{N-2},\psi_{N-1}\} \subset H_0^1(0,1). \tag{3.19}$$

In the appendix we proved the uniform convergence result for a singularly perturbed two point boundary value problem, and showed how the choice of x-transition point and ε-transition point affect the convergence result.

Similarly, for computing the first excited state of BEC with box potential, there is an additional interior layer located at $x=1/2$ with width $\mathcal{O}(2\varepsilon)$, then the partition can be chosen as

$$x_j = x_{j-1} + \begin{cases} h_1, & j\in\{1,N/2,N/2+1,N\}, \\ h_2, & j\in\{2,\cdots,N/2-1\}\cup\{N/2+2,\cdots,N-1\}, \end{cases} \tag{3.20}$$

in which the two kinds of mesh sizes are

$$h_1 = \begin{cases} \min\{\frac{1}{8},\varepsilon\ln N\}, & \varepsilon\le\gamma, \\ \frac{1}{N}, & \varepsilon>\gamma, \end{cases} \qquad h_2 = \frac{1-4h_1}{N-4}, \tag{3.21}$$

and there are four hybrid basis functions $\psi_1,\psi_{N/2-1},\psi_{N/2+1},\psi_{N-1}$ which can be constructed similarly.

For computing the first excited state of BEC with harmonic potential, we take $\Omega=(-c,c)$ and let $-c=x_0<x_1<\cdots<x_N=c$ be its partition. Since there is an interior layer located at $x=0$ with width $\mathcal{O}(2\varepsilon)$, we choose the partition as

$$x_j = x_{j-1} + \begin{cases} h_2, & 1\le j\le N/2-1, \\ h_1, & j=N/2,N/2+1, \\ h_2, & N/2+2\le j\le N, \end{cases} \tag{3.22}$$

in which the two kinds of mesh sizes are

$$h_1 = \begin{cases} \min\{\frac{c}{2},\varepsilon\ln N\}, & \varepsilon\le\gamma, \\ \frac{2c}{N}, & \varepsilon>\gamma, \end{cases} \qquad h_2 = \frac{2c-2h_1}{N-2}, \tag{3.23}$$

and there are two hybrid basis functions $\psi_{N/2-1},\psi_{N/2+1}$ which can be constructed similarly.

Remark 3.1. We make a comparison with our method to other existing numerical methods, especially finite difference method on Shishkin mesh and the tailored finite point method (TFPM) on uniform mesh applied to the BE gradient flow equation (3.6). Shishkin mesh [35,36] is a kind of piecewise uniform mesh. When total $N+1$ points are used, $N/2$ points are located uniformly in the boundary/interior regions and other $N/2$ points are located uniformly in the smooth regions. It has been proved to be uniformly convergent for many singularly perturbed problems. TFPM [27, 28, 30] uses the exact solutions of the local approximated problem as the basis functions, and it can get high accuracy in

https://doi.org/10.4208/cicp.021114.140715a Published online by Cambridge University Press

the regime $0<\varepsilon\ll 1/N$ and $\varepsilon\gg 1/N$. Moreover, if the coefficient functions are piecewise smooth and independent of ε, then TFPM on uniform mesh can be uniformly convergent [29, 31]. However, for our BE gradient flow equation (3.6), the coefficient function $\phi^n(x)$ depends on ε, and its derivatives is not bounded when ε goes to zero. In this case TFPM on uniform mesh can not get satisfactory error estimate result in the regime $\varepsilon=\mathcal{O}(1/N)$, so it is not uniformly convergent for our case.

From the construction of our AFEM-HB we see that AFEM-HB can be considered as a good combination of Shishkin mesh and TFPM. The mesh partition is adapted to the parameter ε. When ε is small, the mesh partition is similar to that of Shishkin mesh, except that only one point is located in every boundary/interior region. The basis functions are chosen to be the same with TFPM in boundary/interior layer regions, and standard piecewise linear basis functions away from the boundary/interior layer regions. When ε is large, our AFEM-HB is reduced to the standard finite element method on uniform mesh. In conclusion, our AFEM-HB is more efficient than the Shishkin mesh method, e.g. half the computational cost, and our AFEM-HB is still uniformly convergent with respect to the mesh size and the parameter ε.

4 Numerical results

In this section, we present numerous numerical examples to show the uniform convergence property of our adaptive finite element method with hybrid basis (AFEM-HB). As we know, classical finite difference/element methods on uniform mesh are not uniformly convergent for singularly perturbed problems [39]. We also compare our AFEM-HB results with that of finite difference method on Shishkin mesh [35, 36] and tailored finite point method (TFPM, [27, 28, 30]) on uniform mesh.

We first show the maximum error results for the singularly perturbed two point boundary value problem for these three methods, then show the maximum error results for the ground and excited states of BEC with box/harmonic potential. After that we will apply the normalized gradient flow combined with our AFEM-HB method to compute the ground and excited states of BEC with box/harmonic/optical lattice potential in the semiclassical regimes ($0<\varepsilon\ll 1$). In our computations, we choose time step $\tau=0.001$, and the stationary state is reached when

$$\max_{0\le i\le N}|\phi_h^{n+1}(x_i)-\phi_h^n(x_i)|<10^{-8}.$$

4.1 Comparison and convergence rate

Example 4.1. In the first example, we compute the maximum errors for the singularly perturbed two point boundary value problem (see the appendix):

$$-\varepsilon^2u''(x)+b(x)u(x)=f(x),x\in(0,1), \tag{4.1}$$

$$u(0)=0,\quad u(1)=0, \tag{4.2}$$

https://doi.org/10.4208/cicp.021114.140715a Published online by Cambridge University Press

where $b(x)=1$ and $f(x)=1+\cos(\pi x)$. It is directly to show that

$$u(x)=1+\frac{\cos(\pi x)}{1+\varepsilon^2\pi^2}+\frac{2+\varepsilon^2\pi^2}{1+\varepsilon^2\pi^2}\cdot\frac{\sinh(\frac{x-1}{\varepsilon})}{\sinh(\frac{1}{\varepsilon})}-\frac{\varepsilon^2\pi^2}{1+\varepsilon^2\pi^2}\cdot\frac{\sinh(\frac{x}{\varepsilon})}{\sinh(\frac{1}{\varepsilon})} \tag{4.3}$$

is the exact solution. Tables 1-3 show the numerical results by using Shishkin mesh, TFPM and AFEM-HB, respectively. Table 4 shows the comparison of these three methods.

From Table 1 we see that the maximum errors by using Shishkin mesh do not increase with $\varepsilon\to 0$, and an essentially second order convergence rate is observed for all $\varepsilon>0$. From Table 2 we see that the maximum errors by using TFPM are very small and decay with $\varepsilon\to 0$ in the region $\varepsilon\ll 1/N$ (i.e. lower triangular part of the table), and second order convergence rate is observed in the region $\varepsilon\gg 1/N$ (i.e. upper triangular part of the table). From Table 3 we see that the maximum errors by using AFEM-HB do not increase significantly with $\varepsilon\to 0$, and second order convergence rate is observed when $\varepsilon\ll 1/N$ or $\varepsilon\gg 1/N$. From Table 4 we see that if we keep $\varepsilon=\mathcal{O}(1/N)$ and let $N\to\infty$, uniformly second order convergent rates are observed by all three methods. For this simple case,

Table 1: Maximum errors, i.e. $\max_{0\le i\le N}|u(x_i)-u_i|$, for Example 4.1 by using Shishkin mesh for different ε and grid points N.

Shishkin mesh	$N_0=2^4$	2^2N_0	2^4N_0	2^6N_0	2^8N_0
$\varepsilon_0=0.1$	1.06E-2	7.03E-4	4.41E-5	2.76E-6	1.73E-7
$\varepsilon_0/2^2$	4.81E-2	8.06E-3	7.43E-4	4.66E-5	2.91E-6
$\varepsilon_0/2^4$	4.81E-2	8.08E-3	9.17E-4	8.98E-5	8.09E-6
$\varepsilon_0/2^6$	4.81E-2	8.08E-3	9.17E-4	8.98E-5	8.09E-6
$\varepsilon_0/2^8$	4.81E-2	8.08E-3	9.17E-4	8.98E-5	8.09E-6
$\varepsilon_0/2^{10}$	4.81E-2	8.08E-3	9.17E-4	8.98E-5	8.09E-6
$\varepsilon_0/2^{12}$	4.81E-2	8.08E-3	9.17E-4	8.98E-5	8.09E-6
$\varepsilon_0/2^{14}$	4.81E-2	8.08E-3	9.17E-4	8.98E-5	8.09E-6

Table 2: Maximum errors, i.e. $\max_{0\le i\le N}|u(x_i)-u_i|$, for Example 4.1 by using TFPM for different ε and grid points N.

TFPM	$N_0=2^4$	2^2N_0	2^4N_0	2^6N_0	2^8N_0
$\varepsilon_0=0.1$	1.95E-3	1.24E-4	7.76E-6	4.85E-7	3.03E-8
$\varepsilon_0/2^2$	2.20E-3	1.83E-4	1.16E-5	7.28E-7	4.55E-8
$\varepsilon_0/2^4$	3.76E-4	1.49E-4	1.22E-5	7.76E-7	4.85E-8
$\varepsilon_0/2^6$	2.36E-5	2.40E-5	9.41E-6	7.68E-7	4.89E-8
$\varepsilon_0/2^8$	1.48E-6	1.50E-6	1.50E-6	5.89E-7	4.81E-8
$\varepsilon_0/2^{10}$	9.23E-8	9.40E-8	9.41E-8	9.37E-8	3.68E-8
$\varepsilon_0/2^{12}$	5.77E-9	5.88E-9	5.88E-9	5.88E-9	5.86E-9
$\varepsilon_0/2^{14}$	3.61E-10	3.67E-10	3.68E-10	3.68E-10	3.68E-10

https://doi.org/10.4208/cicp.021114.140715a Published online by Cambridge University Press

Table 3: Maximum errors, i.e. $\max_{0\le i\le N}|u(x_i)-u_i|$, for Example 4.1 by using AFEM-HB for different ε and grid points N.

AFEM-HB	$N_0=2^4$	2^2N_0	2^4N_0	2^6N_0	2^8N_0
$\varepsilon_0=0.1$	2.68E-2	2.60E-2	3.76E-5	2.65E-6	1.71E-7
$\varepsilon_0/2^2$	4.07E-3	1.41E-3	1.62E-3	3.99E-5	2.80E-6
$\varepsilon_0/2^4$	6.21E-3	3.33E-4	3.98E-5	3.62E-5	3.55E-5
$\varepsilon_0/2^6$	7.23E-3	4.08E-4	2.32E-5	1.77E-6	1.50E-6
$\varepsilon_0/2^8$	7.65E-3	4.53E-4	2.64E-5	1.54E-6	9.05E-8
$\varepsilon_0/2^{10}$	7.77E-3	4.77E-4	2.85E-5	1.69E-6	9.99E-8
$\varepsilon_0/2^{12}$	7.80E-3	4.85E-4	2.98E-5	1.79E-6	1.07E-8
$\varepsilon_0/2^{14}$	7.81E-3	4.88E-4	3.03E-5	1.87E-6	1.13E-7

Table 4: Comparison of the maximum errors for Example 4.1 by using Shishkin mesh, TFPM and AFEM-HB.

N	$N_0=2^4$	2^2N_0	2^4N_0	2^6N_0	2^8N_0
ε	$\varepsilon_0=0.1$	$\varepsilon_0/2^2$	$\varepsilon_0/2^4$	$\varepsilon_0/2^6$	$\varepsilon_0/2^8$
Shishkin mesh	1.06E-2	8.06E-3	9.17E-4	8.98E-5	8.09E-6
TFPM	1.95E-3	1.83E-4	1.22E-5	7.68E-7	4.81E-8
AFEM-HB	2.68E-2	1.41E-3	3.98E-5	1.77E-6	9.05E-8

all the three methods are uniformly convergent with respect to $\varepsilon>0$, and TFPM shows the best numerical results among these three methods. These results are consistent with our theoretical error estimates (A.6), (A.8), (A.25) for the singularly perturbed two point boundary value problem in the appendix.

Example 4.2. In the second example, we compute the maximum errors for the singularly perturbed two point boundary value problem with a more general case. We choose $b(x)=2+x(1-x)$ and

$$f^\varepsilon(x)=(2+x(1-x))(1+\sin^2(\pi x)+e^{-\frac{1}{\varepsilon}})-2\varepsilon^2\pi^2\cos(2\pi x)-(1+x(1-x))(e^{-\frac{x}{\varepsilon}}+e^{-\frac{1-x}{\varepsilon}}).$$

It is easy to check that $u(x)=1+\sin^2(\pi x)+e^{-\frac{1}{\varepsilon}}-e^{-\frac{x}{\varepsilon}}-e^{-\frac{1-x}{\varepsilon}}$ is the exact solution. Tables 5-7 show the results by using Shishkin mesh, TFPM and AFEM-HB, respectively. Table 8 shows the comparison of these three methods.

From Table 6 we see that TFPM has high accuracy in the region $\varepsilon\ll 1/N$ (i.e. lower triangular part of the table), and second order convergence rate is observed in the region $\varepsilon\gg 1/N$ (i.e. upper triangular part of the table). From Table 8 we see that if we keep $\varepsilon=\mathcal{O}(1/N)$ and let $N\to\infty$, then no convergence is observed by using TFPM. From Table 5 and Table 7 we see that Shishkin mesh and AFEM-HB are still uniformly convergent for this general case. Besides, our AFEM-HB shows better results than Shishkin mesh method. These results are consistent with our theoretical error estimates (A.6), (A.8), (A.25) for the singularly perturbed two point boundary value problem in the appendix.

https://doi.org/10.4208/cicp.021114.140715a Published online by Cambridge University Press

Table 5: Maximum errors, i.e. $\max_{0\le i\le N}|u(x_i)-u_i|$, for Example 4.2 by using Shishkin mesh for different ε and grid points N.

Shishkin mesh	$N_0=2^4$	2^2N_0	2^4N_0	2^6N_0	2^8N_0
$\varepsilon_0=0.1$	3.68E-3	2.49E-4	1.56E-5	9.75E-7	6.29E-8
$\varepsilon_0/2^2$	1.49E-2	2.68E-3	2.55E-4	1.60E-5	1.00E-6
$\varepsilon_0/2^4$	1.51E-2	2.70E-3	3.16E-4	3.09E-5	2.78E-6
$\varepsilon_0/2^6$	1.51E-2	2.71E-3	3.16E-4	3.10E-5	2.79E-6
$\varepsilon_0/2^8$	1.51E-2	2.71E-3	3.16E-4	3.10E-5	2.79E-6
$\varepsilon_0/2^{10}$	1.51E-2	2.71E-3	3.16E-4	3.10E-5	2.79E-6
$\varepsilon_0/2^{12}$	1.51E-2	2.71E-3	3.16E-4	3.10E-5	2.79E-6
$\varepsilon_0/2^{14}$	1.51E-2	2.71E-3	3.16E-4	3.10E-5	2.79E-6

Table 6: Maximum errors, i.e. $\max_{0\le i\le N}|u(x_i)-u_i|$, for Example 4.2 by using TFPM for different ε and grid points N.

TFPM	$N_0=2^4$	2^2N_0	2^4N_0	2^6N_0	2^8N_0
$\varepsilon_0=0.1$	4.95E-3	3.28E-4	2.06E-5	1.29E-6	8.06E-8
$\varepsilon_0/2^2$	1.48E-2	3.81E-3	2.61E-4	1.64E-5	1.02E-6
$\varepsilon_0/2^4$	1.71E-4	1.42E-2	3.77E-3	2.57E-4	1.62E-5
$\varepsilon_0/2^6$	1.07E-5	2.24E-5	1.42E-2	3.76E-3	2.57E-4
$\varepsilon_0/2^8$	6.69E-7	6.69E-7	2.20E-5	1.42E-2	3.74E-3
$\varepsilon_0/2^{10}$	4.18E-8	4.18E-8	4.18E-8	2.20E-5	1.42E-2
$\varepsilon_0/2^{12}$	2.61E-9	2.61E-9	2.61E-9	2.61E-9	2.20E-5
$\varepsilon_0/2^{14}$	1.63E-10	1.63E-10	1.63E-10	1.63E-10	1.63E-10

Table 7: Maximum errors, i.e. $\max_{0\le i\le N}|u(x_i)-u_i|$, for Example 4.2 by using AFEM-HB for different ε and grid points N.

AFEM-HB	$N_0=2^4$	2^2N_0	2^4N_0	2^6N_0	2^8N_0
$\varepsilon_0=0.1$	7.63E-2	7.71E-2	1.65E-5	1.04E-6	6.88E-8
$\varepsilon_0/2^2$	3.40E-3	2.96E-3	3.62E-3	1.66E-5	9.13E-7
$\varepsilon_0/2^4$	1.90E-3	1.60E-4	5.21E-5	5.22E-5	6.27E-5
$\varepsilon_0/2^6$	1.89E-3	1.22E-4	9.17E-6	1.83E-6	1.24E-6
$\varepsilon_0/2^8$	1.92E-3	1.22E-4	7.69E-6	5.54E-7	9.45E-8
$\varepsilon_0/2^{10}$	1.94E-3	1.22E-4	7.62E-6	4.81E-7	3.39E-8
$\varepsilon_0/2^{12}$	1.95E-3	1.22E-4	7.63E-6	4.77E-7	3.01E-8
$\varepsilon_0/2^{14}$	1.95E-3	1.22E-4	7.63E-6	4.77E-7	2.98E-8

Example 4.3. In this example we compute the maximum errors for the ground state of BEC with box potential. Let $\phi(x)$ be the numerical 'exact' solution by using Shishkin mesh with $N=2^{16}$, and $\phi^N(x)$ be the numerical solution with $N+1$ grid points. We

https://doi.org/10.4208/cicp.021114.140715a Published online by Cambridge University Press

Table 8: Comparison of the maximum errors for Example 4.2 by using Shishkin mesh, TFPM and AFEM-HB.

N	$N_0=2^4$	2^2N_0	2^4N_0	2^6N_0	2^8N_0
ε	$\varepsilon_0=0.1$	$\varepsilon_0/2^2$	$\varepsilon_0/2^4$	$\varepsilon_0/2^6$	$\varepsilon_0/2^8$
Shishkin mesh	3.68E-3	2.68E-3	3.16E-4	3.10E-5	2.79E-6
TFPM	4.95E-3	3.81E-3	3.77E-3	3.76E-3	3.74E-3
AFEM-HB	7.63E-2	2.96E-3	5.21E-5	1.86E-6	9.45E-8

Table 9: Maximum errors, i.e. $\max_{0\le i\le N}|\phi(x_i)-\phi^N(x_i)|$ for the ground state of BEC with box potential by using Shishkin mesh for different ε and grid points N.

Shishkin mesh	$N_0=2^4$	2^2N_0	2^4N_0	2^6N_0	2^8N_0
$\varepsilon_0=0.1$	2.64E-2	1.70E-3	1.06E-4	6.58E-6	4.57E-7
$\varepsilon_0/2^2$	2.72E-2	4.01E-3	4.42E-4	4.32E-5	3.62E-6
$\varepsilon_0/2^4$	2.70E-2	3.84E-3	4.27E-4	4.16E-5	3.68E-6
$\varepsilon_0/2^6$	2.70E-2	3.81E-3	4.23E-4	4.12E-5	5.76E-6
$\varepsilon_0/2^8$	2.69E-2	3.78E-3	4.22E-4	4.27E-5	5.71E-6
$\varepsilon_0/2^{10}$	2.69E-2	3.78E-3	4.22E-4	4.27E-5	5.71E-6
$\varepsilon_0/2^{12}$	2.70E-2	3.78E-3	4.22E-4	4.27E-5	5.71E-6
$\varepsilon_0/2^{14}$	2.70E-2	3.78E-3	4.22E-4	4.27E-5	5.71E-6

Table 10: Maximum errors, i.e. $\max_{0\le i\le N}|\phi(x_i)-\phi^N(x_i)|$ for the ground state of BEC with box potential by using TFPM for different ε and grid points N.

TFPM	$N_0=2^4$	2^2N_0	2^4N_0	2^6N_0	2^8N_0
$\varepsilon_0=0.1$	3.02E-2	2.97E-3	1.91E-4	1.20E-5	7.76E-7
$\varepsilon_0/2^2$	7.48E-3	2.69E-2	2.31E-3	1.47E-4	9.51E-6
$\varepsilon_0/2^4$	2.69E-3	3.69E-3	2.60E-2	2.17E-3	1.37E-4
$\varepsilon_0/2^6$	6.90E-4	6.68E-4	4.05E-3	2.58E-2	2.13E-3
$\varepsilon_0/2^8$	1.72E-4	1.70E-4	1.65E-4	4.14E-3	2.58E-2
$\varepsilon_0/2^{10}$	4.01E-5	4.00E-5	3.97E-5	3.87E-5	4.16E-3
$\varepsilon_0/2^{12}$	1.10E-5	1.10E-5	1.10E-5	1.09E-5	1.05E-5
$\varepsilon_0/2^{14}$	2.78E-6	2.78E-6	2.78E-6	2.78E-6	2.76E-6

compute the maximum errors, i.e. $\max_{0\le i\le N}|\phi(x_i)-\phi^N(x_i)|$ for the ground state of BEC with box potential. Tables 9-11 show the results by using Shishkin mesh, TFPM and AFEM-HB, respectively. Table 12 shows the comparison of these three methods.

From Tables 9-12, similar conclusions as those for the singularly perturbed two point boundary value problem can be drawn.

Example 4.4. In this example we compute the first excited state of BEC with box potential. Tables 13-15 show the results by using Shishkin mesh, TFPM and AFEM-HB, respectively.

https://doi.org/10.4208/cicp.021114.140715a Published online by Cambridge University Press

Table 11: Maximum errors, i.e. $\max_{0\le i\le N}|\phi(x_i)-\phi^N(x_i)|$ for the ground state of BEC with box potential by using AFEM-HB for different ε and grid points N.

AFEM-HB	$N_0=2^4$	2^2N_0	2^4N_0	2^6N_0	2^8N_0
$\varepsilon_0=0.1$	3.70E-4	2.16E-5	2.04E-4	8.08E-6	4.51E-7
$\varepsilon_0/2^2$	2.55E-3	2.85E-5	1.20E-7	2.18E-8	6.97E-6
$\varepsilon_0/2^4$	5.86E-3	1.44E-4	2.52E-6	2.54E-8	2.71E-8
$\varepsilon_0/2^6$	7.25E-3	3.21E-4	1.03E-5	1.82E-7	2.69E-8
$\varepsilon_0/2^8$	7.64E-3	4.36E-4	1.77E-5	7.02E-7	2.54E-8
$\varepsilon_0/2^{10}$	7.75E-3	4.74E-4	2.61E-5	9.90E-7	4.66E-8
$\varepsilon_0/2^{12}$	7.77E-3	4.85E-4	2.93E-5	1.56E-6	5.59E-8
$\varepsilon_0/2^{14}$	7.78E-3	4.87E-4	3.02E-5	1.81E-6	9.39E-8

Table 12: Comparison of the maximum errors for the ground state of BEC with box potential by using Shishkin mesh, TFPM and AFEM-HB.

N	$N_0=2^4$	2^2N_0	2^4N_0	2^6N_0	2^8N_0
ε	$\varepsilon_0=0.1$	$\varepsilon_0/2^2$	$\varepsilon_0/2^4$	$\varepsilon_0/2^6$	$\varepsilon_0/2^8$
Shishkin mesh	2.64E-2	4.01E-3	4.27E-4	4.12E-5	5.71E-6
TFPM	3.02E-2	2.69E-2	2.60E-2	2.58E-2	2.58E-2
AFEM-HB	3.70E-4	2.85E-5	2.52E-6	1.82E-7	2.54E-8

Table 13: Maximum errors for the first excited state of BEC with box potential by using Shishkin mesh for different ε and grid points N.

Shishkin mesh	$N_0=2^4$	2^2N_0	2^4N_0	2^6N_0	2^8N_0
$\varepsilon_0=0.1$	3.84E-2	2.51E-3	1.57E-4	9.87E-6	6.75E-7
$\varepsilon_0/2^2$	1.84E-1	1.86E-2	1.52E-3	9.50E-5	5.61E-6
$\varepsilon_0/2^4$	1.66E-1	1.69E-2	1.66E-3	1.52E-4	1.40E-5
$\varepsilon_0/2^6$	1.61E-1	1.66E-2	1.62E-3	1.50E-4	1.46E-5
$\varepsilon_0/2^8$	1.60E-1	1.65E-2	1.62E-3	1.50E-4	1.45E-5
$\varepsilon_0/2^{10}$	1.60E-1	1.65E-2	1.60E-3	1.49E-4	1.45E-5
$\varepsilon_0/2^{12}$	1.60E-1	1.64E-2	1.63E-3	1.49E-4	1.45E-5
$\varepsilon_0/2^{14}$	1.60E-1	1.64E-2	1.63E-3	1.49E-4	1.45E-5

Table 16 shows the comparison of these three methods. Similar conclusions as those for the ground state of BEC with box potential can be drawn.

Example 4.5. In this example we compute the first excited state of BEC with harmonic potential. Tables 17-19 show the results by using Shishkin mesh, TFPM and AFEM-HB, respectively. Table 20 shows the comparison of these three methods.

From Tables 17-19 we see that these methods converges slower than the previous three examples. The maximum errors even increase when $\varepsilon\to 0$ for all these three meth-

https://doi.org/10.4208/cicp.021114.140715a Published online by Cambridge University Press

Table 14: Maximum errors for the first excited state of BEC with box potential by using TFPM for different ε and grid points N.

TFPM	$N_0=2^4$	2^2N_0	2^4N_0	2^6N_0	2^8N_0
$\varepsilon_0=0.1$	3.52E-2	4.05E-3	2.68E-4	1.70E-5	1.10E-6
$\varepsilon_0/2^2$	3.60E-3	2.81E-2	2.52E-3	1.61E-4	1.04E-5
$\varepsilon_0/2^4$	5.40E-3	4.02E-3	2.63E-2	2.22E-3	1.41E-4
$\varepsilon_0/2^6$	1.39E-3	1.34E-3	3.93E-3	2.58E-2	2.21E-3
$\varepsilon_0/2^8$	3.46E-4	3.44E-4	3.33E-4	4.11E-3	2.57E-2
$\varepsilon_0/2^{10}$	8.50E-5	8.51E-5	8.45E-5	8.15E-5	4.16E-3
$\varepsilon_0/2^{12}$	1.98E-5	2.00E-5	1.97E-5	1.98E-5	1.89E-5
$\varepsilon_0/2^{14}$	4.02E-6	4.30E-6	4.00E-6	3.74E-6	3.79E-6

Table 15: Maximum errors for the first excited state of BEC with box potential by using AFEM-HB for different ε and grid points N.

AFEM-HB	$N_0=2^4$	2^2N_0	2^4N_0	2^6N_0	2^8N_0
$\varepsilon_0=0.1$	6.10E-3	3.22E-4	2.68E-4	1.70E-5	1.07E-6
$\varepsilon_0/2^2$	2.06E-3	1.64E-5	1.71E-7	2.27E-8	8.56E-6
$\varepsilon_0/2^4$	4.44E-3	1.58E-4	2.10E-6	5.00E-8	4.21E-8
$\varepsilon_0/2^6$	6.74E-3	2.06E-4	1.10E-5	2.03E-7	3.87E-8
$\varepsilon_0/2^8$	7.50E-3	3.78E-4	1.47E-5	7.60E-7	5.06E-8
$\varepsilon_0/2^{10}$	7.71E-3	4.56E-4	2.14E-5	1.04E-6	8.25E-8
$\varepsilon_0/2^{12}$	7.76E-3	4.80E-4	2.77E-5	1.19E-6	1.01E-7
$\varepsilon_0/2^{14}$	7.77E-3	4.86E-4	2.98E-5	1.68E-6	7.41E-8

Table 16: Comparison of the maximum errors for the first excited state of BEC with box potential by using Shishkin mesh, TFPM and AFEM-HB.

N	$N_0=2^4$	2^2N_0	2^4N_0	2^6N_0	2^8N_0
ε	$\varepsilon_0=0.1$	$\varepsilon_0/2^2$	$\varepsilon_0/2^4$	$\varepsilon_0/2^6$	$\varepsilon_0/2^8$
Shishkin mesh	3.84E-2	1.86E-2	1.66E-3	1.50E-4	1.45E-5
TFPM	3.52E-2	2.81E-2	2.63E-2	2.58E-2	2.57E-2
AFEM-HB	6.10E-3	1.64E-5	2.10E-6	2.03E-7	5.06E-8

ods. In Table 20 we see that both Shishkin mesh and AFEM-HB are uniformly convergent, but only first convergence rates are observed. This is due to the fast descent near $x=\pm\sqrt{2\mu}$ when $\varepsilon\to 0$. But later in Example 4.7 we will see that the errors near the interior layer do not increase as $\varepsilon\to 0$. So our AFEM-HB is still uniformly convergent and can capture the boundary/interior layers accurately for all $\varepsilon>0$.

https://doi.org/10.4208/cicp.021114.140715a Published online by Cambridge University Press

Table 17: Maximum errors for the first excited state of BEC with harmonic potential by using Shishkin mesh for different ε and grid points N.

Shishkin mesh	$N_0=2^4$	2^2N_0	2^4N_0	2^6N_0	2^8N_0
$\varepsilon_0=0.1$	6.71E-2	2.72E-3	2.41E-4	2.35E-5	2.11E-6
$\varepsilon_0/2^2$	1.72E-1	1.63E-2	9.83E-4	5.88E-5	3.65E-6
$\varepsilon_0/2^4$	2.27E-1	5.73E-2	4.06E-3	2.76E-4	1.74E-5
$\varepsilon_0/2^6$	2.54E-1	9.47E-2	1.18E-2	1.13E-3	7.30E-5
$\varepsilon_0/2^8$	2.65E-1	1.12E-1	2.54E-2	4.17E-3	2.85E-4
$\varepsilon_0/2^{10}$	2.70E-1	1.20E-1	3.76E-2	1.10E-2	1.26E-3
$\varepsilon_0/2^{12}$	2.72E-1	1.22E-1	4.27E-2	1.60E-2	3.48E-3
$\varepsilon_0/2^{14}$	2.72E-1	1.22E-1	4.35E-2	1.67E-2	4.11E-3

Table 18: Maximum errors for the first excited state of BEC with harmonic potential by using TFPM for different ε and grid points N.

TFPM	$N_0=2^4$	2^2N_0	2^4N_0	2^6N_0	2^8N_0
$\varepsilon_0=0.1$	4.33E-2	1.59E-2	8.05E-4	4.70E-5	2.94E-6
$\varepsilon_0/2^2$	2.65E-2	3.81E-2	1.43E-2	7.26E-4	4.28E-5
$\varepsilon_0/2^4$	9.00E-2	2.28E-2	4.00E-2	1.39E-2	7.07E-4
$\varepsilon_0/2^6$	1.30E-1	5.74E-2	1.20E-2	4.06E-2	1.38E-2
$\varepsilon_0/2^8$	1.49E-1	8.01E-2	2.05E-2	1.21E-2	4.07E-2
$\varepsilon_0/2^{10}$	1.58E-1	9.07E-2	3.38E-2	5.11E-2	1.21E-2
$\varepsilon_0/2^{12}$	1.61E-1	9.42E-2	3.90E-2	8.91E-3	2.84E-3
$\varepsilon_0/2^{14}$	1.61E-1	9.48E-2	3.98E-2	9.68E-3	6.98E-4

Table 19: Maximum errors for the first excited state of BEC with harmonic potential by using AFEM-HB for different ε and grid points N.

AFEM-HB	$N_0=2^4$	2^2N_0	2^4N_0	2^6N_0	2^8N_0
$\varepsilon_0=0.1$	2.30E-2	4.41E-2	8.12E-4	4.70E-5	2.94E-6
$\varepsilon_0/2^2$	6.15E-2	5.58E-3	5.74E-3	5.76E-3	4.28E-5
$\varepsilon_0/2^4$	9.09E-2	8.77E-3	1.30E-3	1.48E-3	1.67E-3
$\varepsilon_0/2^6$	8.80E-2	1.32E-2	3.69E-3	3.00E-4	3.15E-4
$\varepsilon_0/2^8$	8.64E-2	3.27E-2	5.42E-3	1.08E-3	7.27E-5
$\varepsilon_0/2^{10}$	8.64E-2	4.47E-2	1.42E-2	3.49E-3	3.33E-4
$\varepsilon_0/2^{12}$	8.73E-2	4.91E-2	1.96E-2	6.71E-3	9.14E-4
$\varepsilon_0/2^{14}$	8.75E-2	4.98E-2	2.05E-2	7.52E-3	1.24E-3

4.2 Application to BEC

Example 4.6. We compute the ground and excited states of BEC with box potential in 1D.

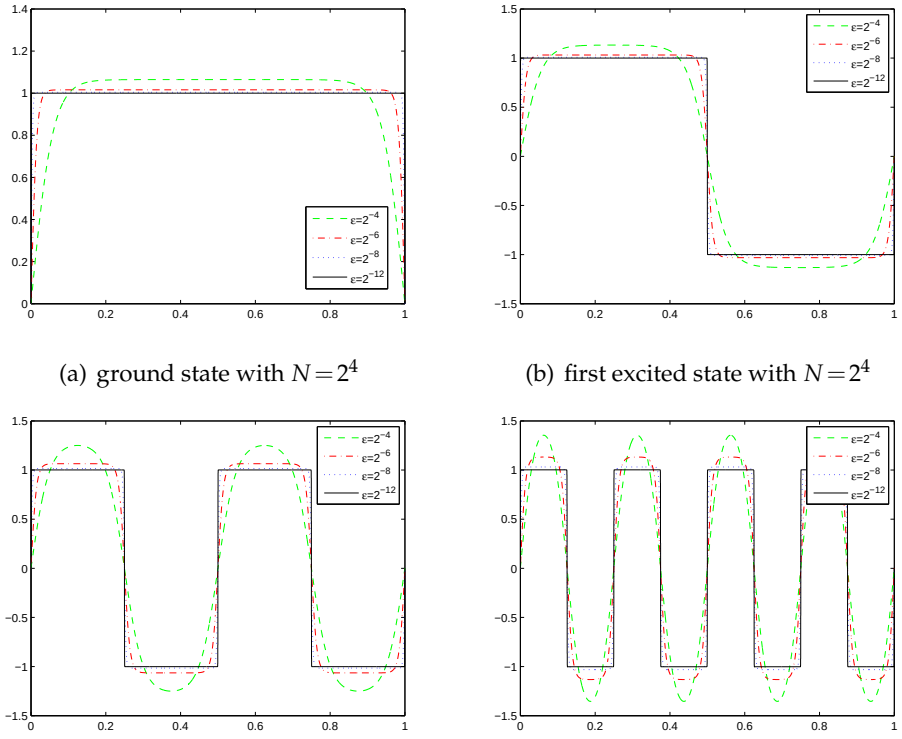
https://doi.org/10.4208/cicp.021114.140715a Published online by Cambridge University Press

Table 20: Comparison of the maximum errors for the first excited state of BEC with harmonic potential by using Shishkin mesh, TFPM and AFEM-HB.

N	$N_0=2^4$	2^2N_0	2^4N_0	2^6N_0	2^8N_0
ε	$\varepsilon_0=0.1$	$\varepsilon_0/2^2$	$\varepsilon_0/2^4$	$\varepsilon_0/2^6$	$\varepsilon_0/2^8$
Shishkin mesh	6.71E-2	1.63E-2	4.06E-3	1.13E-3	2.85E-4
TFPM	4.33E-2	3.81E-2	4.00E-2	4.06E-2	4.07E-2
AFEM-HB	2.30E-2	5.58E-3	1.30E-3	3.00E-4	7.27E-5

Fig. 1 shows the ground and excited states for different ε. We see that boundary layers are observed both in ground state and all excited states, and interior layers are observed in excited states when ε is small, which agree well with the asymptotic results in Section 2. Table 21 lists their corresponding energy and chemical potential. It shows that if all different eigenfunctions of the nonlinear eigenvalue problem are ranked according to their energy, then the corresponding eigenvalues are in the same rank, i.e.

$$E(\phi_g)<E(\phi_1)<\cdots<E(\phi_k)<\cdots \implies \mu(\phi_g)<\mu(\phi_1)<\cdots<\mu(\phi_k)<\cdots, \tag{4.4}$$



(a) ground state with $N=2^4$ (b) first excited state with $N=2^4$

(c) third excited state with $N=2^5$ (d) seventh excited state with $N=2^8$

Figure 1: Ground and excited states of BEC with box potential in 1D for different ε by AFEM-HB.

https://doi.org/10.4208/cicp.021114.140715a Published online by Cambridge University Press

Table 21: Energy and chemical potential for the ground state and excited states of BEC with box potential by using AFEM-HB with different small ε.

ε	2^{-2}	2^{-4}	2^{-6}	2^{-8}	2^{-10}	2^{-12}
E_g	1.0082	0.5918	0.5213	0.5052	0.5013	0.5003
E_1	2.0904	0.7037	0.5437	0.5105	0.5026	0.5007
E_3	5.6779	0.9950	0.5917	0.5213	0.5052	0.5013
E_7	20.476	1.9620	0.7022	0.5437	0.5105	0.5026
μ_g	1.6952	1.1361	1.0319	1.0079	1.0020	1.0005
μ_1	2.8923	1.2963	1.0652	1.0158	1.0039	1.0010
μ_3	6.4159	1.6413	1.1331	1.0317	1.0078	1.0020
μ_7	21.223	2.6722	1.2832	1.0645	1.0157	1.0039

and in the limiting case $\varepsilon \to 0$ we have

$$\lim_{\varepsilon\to 0} E(\phi_g) = \lim_{\varepsilon\to 0} E(\phi_k) = \frac{1}{2}, \quad \lim_{\varepsilon\to 0} \mu(\phi_g) = \lim_{\varepsilon\to 0} \mu(\phi_k) = 1. \tag{4.5}$$

Example 4.7. We compute the first excited state of BEC with harmonic potential in 1D.

Fig. 2 shows the first excited state for different ε and the nodes error distribution by using AFEM-HB. We see that interior layer is observed in the first excited state when ε is small, which agrees well with the asymptotic results in Section 2. The errors are mainly distributed near $x = \pm\sqrt{2\mu}$ due to the fast descent of the solution. The errors in the interior region $x \approx 0$ are relatively smaller. So our AFEM-HB can capture the rapid transition near the boundary/interior layers. Table 22 lists their corresponding energy and chemical potential. It agrees well with that given by the Thomas-Fermi approximation results.

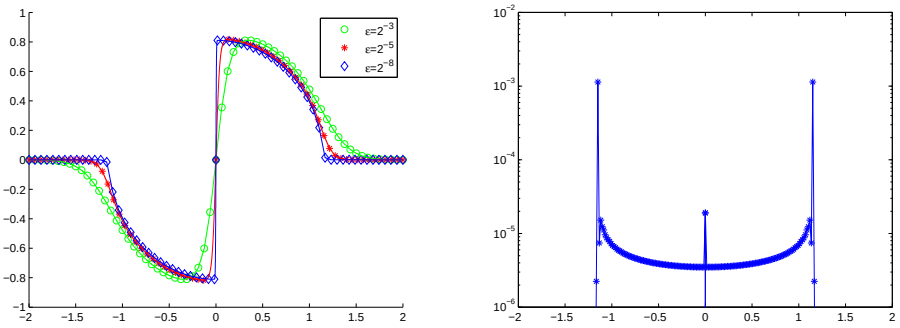
$$\lim_{\varepsilon\to 0} E(\phi_g) = \lim_{\varepsilon\to 0} E(\phi_1) = \frac{3}{10}\left(\frac{3}{2}\right)^{\frac{2}{3}} = 0.3931, \tag{4.6}$$

$$\lim_{\varepsilon\to 0} \mu(\phi_g) = \lim_{\varepsilon\to 0} \mu(\phi_1) = \frac{1}{2}\left(\frac{3}{2}\right)^{\frac{2}{3}} = 0.6552. \tag{4.7}$$

Table 22: Energy and chemical potential for the ground state and first excited state of BEC with harmonic potential by using AFEM-HB with different small ε.

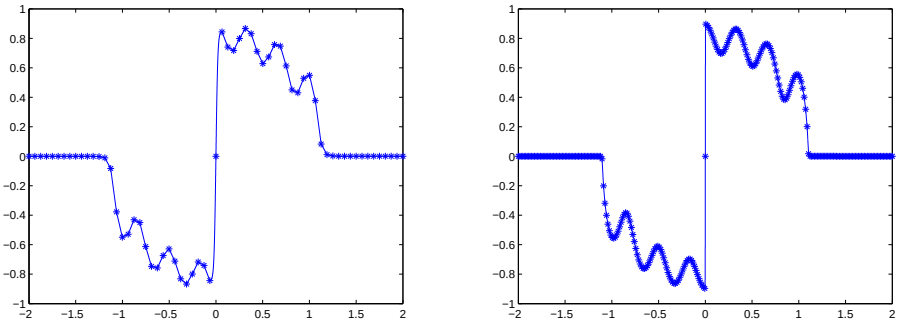
ε	2^{-2}	2^{-4}	2^{-6}	2^{-8}	2^{-10}	2^{-12}
E_g	0.4271	0.3962	0.3934	0.3931	0.3931	0.3931
E_1	0.6354	0.4431	0.4050	0.3961	0.3939	0.3934
μ_g	0.6739	0.6567	0.6553	0.6552	0.6552	0.6552
μ_1	0.8658	0.7024	0.6661	0.6577	0.6559	0.6554

https://doi.org/10.4208/cicp.021114.140715a Published online by Cambridge University Press



(a) first excited state with $N=2^6$ (b) error distribution with $\varepsilon=0.1\times 2^{-10}, N=2^8$

Figure 2: First excited state of BEC with harmonic potential in 1D by using AFEM-HB.



(a) first excited state with $N=2^6, \varepsilon=2^{-6}$ (b) first excited state with $N=2^8, \varepsilon=2^{-10}$

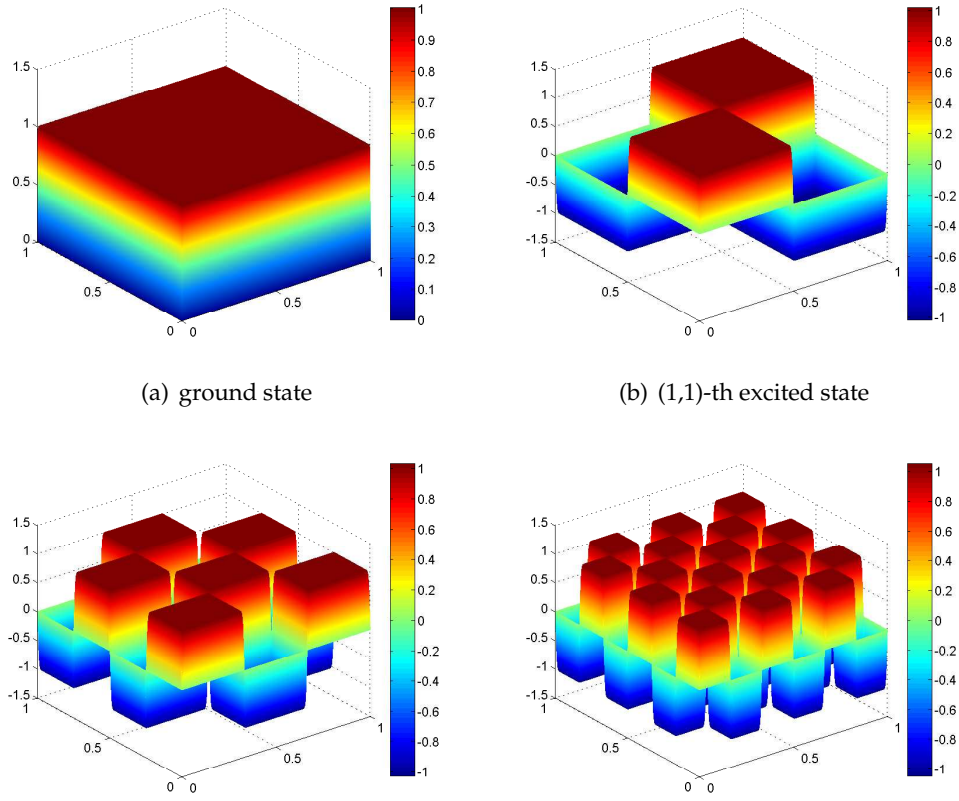
Figure 3: First excited state of BEC with optical lattice potential $V(x)=x^2/2+0.3\sin^2(3\pi x)$ in 1D by using AFEM-HB.

Example 4.8. We compute the first excited state of BEC with optical lattice potential in 1D. Fig. 3 shows the first excited state for different ε. Similar conclusions as those for BEC with harmonic potential in 1D can be drawn.

Example 4.9. We compute the ground and excited states of BEC with box potential in 2D. Fig. 4 shows surface plots for ground and $(1,1)$, $(2,3)$, $(5,5)$-th excited states of BEC with box potential in 2D when $\varepsilon=2^{-10}$ over a 100×100 mesh. It agrees well with the asymptotic solutions given in Section 2.

Example 4.10. We compute the ground and excited states of BEC with harmonic potential in 2D. Fig. 5 shows surface plots for ground and $(1,0)$, $(0,1)$, $(1,1)$-th excited states of BEC with harmonic potential in 2D when $\varepsilon=2^{-10}$ over a 100×100 mesh. It agrees well with the asymptotic solutions given in Section 2.

https://doi.org/10.4208/cicp.021114.140715a Published online by Cambridge University Press



(a) ground state (b) (1,1)-th excited state

(c) (2,3)-th excited state (d) (5,5)-th excited state

Figure 4: Ground and excited states of BEC with box potential in 2D when $\varepsilon=2^{-10}$ over a 100×100 mesh.

Appendix: Uniform convergence of AFEM-HB for a singularly perturbed two point boundary value problem

In this appendix we show that our adaptive finite element method with hybrid basis (AFEM-HB) is uniformly convergent for the following two point boundary value problem:

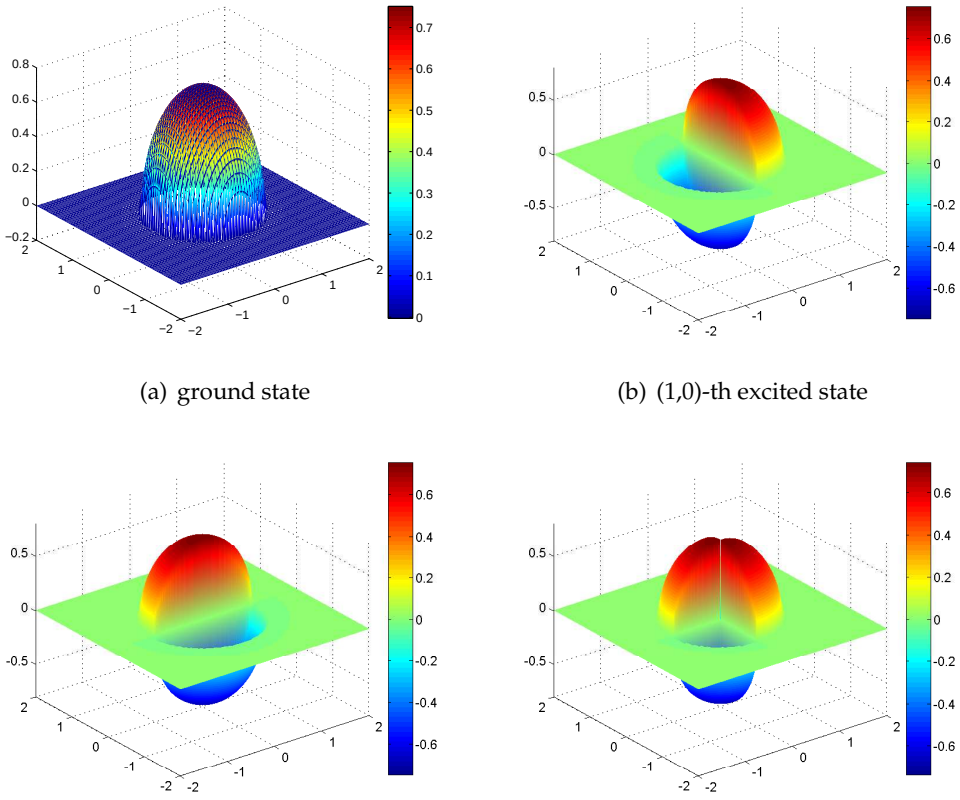
$$-\varepsilon^2 u''(x)+b(x)u(x)=f(x), \quad x\in(0,1), \tag{A.1}$$

$$u(0)=0, \quad u(1)=0, \tag{A.2}$$

where the functions $b(x),f(x)\in C^4[0,1]$ independent of ε and $0<\varepsilon\leq 1$. It is assumed furthermore that the coefficient function satisfies the condition

$$b(x)\geq\beta^2>0 \ \text{ with } \ \beta>0, \quad \text{for all } \ x\in[0,1], \tag{A.3}$$

https://doi.org/10.4208/cicp.021114.140715a Published online by Cambridge University Press



(a) ground state (b) (1,0)-th excited state

(c) (0,1)-th excited state (d) (1,1)-th excited state

Figure 5: Ground and excited states of BEC with harmonic potential in 2D when $\varepsilon=2^{-10}$ over a 100×100 mesh.

then we have the following estimates for the solution $u(x)$ and its derivatives:

$$|u^{(j)}(x)|\leq C(1+\varepsilon^{-j}e^{-\frac{\beta x}{\varepsilon}}+\varepsilon^{-j}e^{-\frac{\beta(1-x)}{\varepsilon}}),\quad j=0,\cdots,4. \tag{A.4}$$

This problem is a singular perturbation problem when $\varepsilon\ll1$. It is somewhat similar to Eq. (3.6) where we applied the normalized gradient flow method with semi-implicit backward Euler discretization in time to the nonlinear eigenvalue problem (1.1)-(1.3). If $f(0)$ and $f(1)$ are not zero, then boundary layers will appear near $x=0$ and $x=1$. Denote $\mu_0=\sqrt{b(0)}/\varepsilon$ and $\mu_1=\sqrt{b(1)}/\varepsilon$, the matched asymptotic expansion gives the asymptotic solution:

$$u^{MA}(x)=\frac{f(x)}{b(x)}-\frac{f(0)}{b(0)}\frac{\sinh(\mu_0(1-x))}{\sinh(\mu_0)}-\frac{f(1)}{b(1)}\frac{\sinh(\mu_1 x)}{\sinh(\mu_1)}. \tag{A.5}$$

It has two boundary layers near $x=0$ and $x=1$ with width $\mathcal{O}(\varepsilon)$.

https://doi.org/10.4208/cicp.021114.140715a Published online by Cambridge University Press

Let $0=x_0<x_1<\cdots<x_N=1$ be a partition of the interval $[0,1]$. It is known that classical finite difference/element methods on uniform mesh are not uniformly convergent for the singularly perturbed problem (A.1)-(A.2). Some special techniques are needed in order to have good convergence property [39]. For example, we use finite difference method on Shishkin mesh (also known as piecewise uniform mesh, layer-adapted mesh [35,36]), then we have the essentially second order maximum error estimate (see [35], Chapter 6):

$$\max_{0\le i\le N}|u_i-u(x_i)|\le C(N^{-1}\ln N)^2. \tag{A.6}$$

There are some special schemes on uniform mesh, for example, the tailored finite point method (TFPM [29,31]), is at least uniform first order for this problem (see [31], Theorem 4.1):

$$\max_{0\le i\le N}|u_i-u(x_i)|\le C/N. \tag{A.7}$$

However, in some cases, while the solution $u(x)$ satisfies the estimate (A.4), the coefficient functions $b(x)$ and $f(x)$ may be dependent of ε and their derivatives may be infinity when ε goes to zero. For example, in the BE gradient flow equation (3.6) we have $f^\varepsilon(x)=\phi^n(x)$, and it behaves the same boundary/interior layers with the ground/excited state $\phi^\varepsilon(x)$. In this case, the maximum error estimate of TFPM applied to the singularly perturbed problem (A.1)-(A.2) is (see [27], Theorem 4.2):

$$\max_{0\le i\le N}|u_i-u(x_i)|\le C\varepsilon^2+Ce^{-\frac{\beta}{\varepsilon N}},\quad \varepsilon\ll 1/N. \tag{A.8}$$

So TFPM can still have high accuracy on coarse mesh when $0<\varepsilon\ll 1$, but now TFPM is not uniformly convergent for all $\varepsilon>0$ in this case. There are also some uniformly convergent schemes on uniform mesh [38,39] for this singularly perturbed problem (A.1)-(A.2), but the frameworks are strongly problem determined and people did not get uniformly convergent result even in higher dimensions. We hope to find a method that is uniformly convergent and easy to extend to other singularly perturbed problems.

Since we have known the locations and widths of the boundary layers, and the asymptotic behaviors in the boundary layer regions, the natural way is to use the asymptotic solution to be the basis functions in boundary layer regions, and use polynomial functions to be the basis functions in smooth regions. We call it the "adaptive finite element method with hybrid basis", and expect it to be uniformly convergent even with the finest mesh size much greater than $\mathcal{O}(\varepsilon)$.

For simplicity of notation, we introduce the method in one dimension. Generalizations to higher dimensions are straightforward for tensor products grids. Let $0=x_0<x_1<\cdots<x_N=1$ be a partition of the interval $[0,1]$, we set

$$x_j=x_{j-1}+\begin{cases} h_1, & j=1,\\ h_2, & 2\le j\le N-1,\\ h_1, & j=N,\end{cases} \tag{A.9}$$

https://doi.org/10.4208/cicp.021114.140715a Published online by Cambridge University Press

in which the two kinds of mesh sizes are

$$h_1=\begin{cases}\sigma, & \varepsilon\le\gamma,\\ \frac{1}{N}, & \varepsilon>\gamma,\end{cases}\qquad h_2=\frac{1-2h_1}{N-2}. \tag{A.10}$$

Here we call $\sigma=\min\{\frac{1}{4},\frac{2}{\beta}\varepsilon\ln N\}$ the x-transition point and $\gamma=(\ln N)^{\frac{1}{3}}/N^{\frac{2}{3}}$ the ε-transition point. When $\varepsilon\le\gamma$, $[0,\sigma]$ and $[1-\sigma,1]$ are the two boundary layers regions, and the outer is the smooth region. We note that we take only one point in every boundary layer region, and the mesh size is much greater than ε. When $\varepsilon>\gamma$, the mesh is an uniform partition, and classical finite difference/element methods can work well.

Now we come to construct the hybrid finite element space V_h. Let $\{\phi_i\}_{i=2}^{N-2}$ be the standard piecewise linear hat functions that satisfy $\phi_i(x_j)=\delta_{ij}$ for $j=0,1,\cdots,N$. We make use of the asymptotic solution (A.5) and let the other two hybrid basis functions ϕ_1 and ϕ_{N-1} be

$$\phi_1(x)=\begin{cases}1-\frac{\sinh(\mu_0(x_1-x))}{\sinh(\mu_0 h_1)}, & x\in[x_0,x_1),\\ \frac{x_2-x}{x_2-x_1}, & x\in[x_1,x_2),\\ 0, & \text{otherwise},\end{cases} \tag{A.11}$$

$$\phi_{N-1}(x)=\begin{cases}1-\frac{\sinh(\mu_1(x-x_{N-1}))}{\sinh(\mu_1 h_1)}, & x\in(x_{N-1},x_N],\\ \frac{x-x_{N-2}}{x_{N-1}-x_{N-2}}, & x\in(x_{N-2},x_{N-1}],\\ 0, & \text{otherwise}.\end{cases} \tag{A.12}$$

The hybrid finite element space is

$$V_h:=\text{span}\{\phi_1,\phi_2,\cdots,\phi_{N-2},\phi_{N-1}\}\subset H_0^1(0,1). \tag{A.13}$$

The finite element approximation of (A.1)-(A.2) is to find $u_h(x)=\sum_{i=1}^{N-1}u_i\phi_i(x)$ such that

$$\varepsilon^2(u_{h,x},v_{h,x})+(b\cdot u_h,v_h)=(f,v_h),\quad \forall v_h\in V_h. \tag{A.14}$$

Since it is not easy to find the interpolation error estimate for this hybrid element, we write it in a difference form with proper numerical integration, and use the discrete maximum principle to give an uniformly point-wise estimate. The error analysis depends on whether ε is less or greater than the ε-transition point γ.

Case 1: $\varepsilon\le\gamma$**.** When ε is less than the ε-transition point γ, the difference form of (A.14) with proper numerical integration in the smooth region $[x_1,x_{N-1}]$ is

$$-\varepsilon^2\frac{u_{i+1}-2u_i+u_{i-1}}{h_2}+h_2\cdot b_i\cdot u_i=h_2\cdot f_i,\quad i=2,\cdots,N-2. \tag{A.15}$$

We compute the truncation error is

$$T(x_i)=-\varepsilon^2\frac{u(x_{i+1})-2u(x_i)+u(x_{i-1})}{h_2^2}+b_i\cdot u(x_i)-f_i. \tag{A.16}$$

https://doi.org/10.4208/cicp.021114.140715a Published online by Cambridge University Press

By Taylor's expansion and Eq. (A.4), we have

$$|T(x_i)| \le C\varepsilon^2 \max_{x\in[x_1,x_{N-1}]} |u^{(2)}(x)| \le C\left(\varepsilon^2 + \frac{1}{N^2}\right). \tag{A.17}$$

The difference form of (A.14) with proper numerical integration in the left boundary region $[x_0,x_2]$ is a hybrid scheme

$$\begin{aligned} &-\varepsilon^2 \frac{u_2-u_1}{h_2} + \varepsilon^2\mu_0 \frac{u_1-u_0}{\sinh(\mu_0 h_1)} + \left(h_1 - \frac{\cosh(\mu_0 h_1)-1}{\mu_0 \sinh(\mu_0 h_1)} + \frac{h_2}{2}\right)\cdot b_1 \cdot u_1 \\ &= \left(h_1 - \frac{\cosh(\mu_0 h_1)-1}{\mu_0 \sinh(\mu_0 h_1)} + \frac{h_2}{2}\right)\cdot f_1. \end{aligned} \tag{A.18}$$

We know

$$\left|\frac{u(x_2)-u(x_1)}{h_2}\right| = \left|\frac{1}{h_2}\int_{x_1}^{x_2} u'(x)dx\right| \le C(1+\varepsilon^{-1}e^{-\frac{\beta h_1}{\varepsilon}}) \le C\left(1+\frac{1}{\varepsilon N^2}\right), \tag{A.19}$$

then the truncation error at the point x_1 is bounded by

$$\begin{aligned} |T(x_1)| &\le \frac{C\varepsilon^2}{h_1+h_2}\left|\frac{u(x_2)-u(x_1)}{h_2}\right| + \frac{C\varepsilon^2\mu_0|u(x_1)|}{\sinh(\mu_0 h_1)(h_1+h_2)} + \varepsilon^2|u''(x_1)| \\ &\le \frac{C}{N^2} + \frac{C\varepsilon^2}{h_1+h_2} + C\varepsilon^2. \end{aligned} \tag{A.20}$$

Since $\varepsilon \le \gamma$, we have $|T(x_1)| \le C/(N\ln N)^{\frac{2}{3}}$. We have the same estimate for $T(x_{N-1})$. So when $\varepsilon \le \gamma$ the truncation error is uniformly bounded by

$$|T(x_i)| \le \frac{C}{(N\ln N)^{\frac{2}{3}}}, \qquad i=1,2,\cdots,N-1. \tag{A.21}$$

Case 2: $\varepsilon > \gamma$**.** When ε is greater than the ε-transition point γ, we have the uniform mesh with $h_1=h_2=h=\frac{1}{N}$. The difference form of (A.14) with proper numerical integration is

$$-\varepsilon^2 \frac{u_{i+1}-2u_i+u_{i-1}}{h} + h\cdot b_i \cdot u_i = h\cdot f_i, \quad i=1,\cdots,N-1. \tag{A.22}$$

The truncation error is

$$\begin{aligned} T(x_i) &= -\varepsilon^2 \frac{u(x_{i+1})-2u(x_i)+u(x_{i-1})}{h^2} + b_i\cdot u(x_i) - f_i \\ &= -\frac{1}{12}\varepsilon^2 h^2 u^{(4)}(x_i) + \mathcal{O}\left(\frac{h^4}{\varepsilon^4}\right), \end{aligned} \tag{A.23}$$

so by the estimate (A.4) we get the truncation error bounded by

$$|T(x_i)| \le C\frac{h^2}{\varepsilon^2} \le \frac{C}{(N\ln N)^{\frac{2}{3}}}, \qquad i=1,2,\cdots,N-1. \tag{A.24}$$

https://doi.org/10.4208/cicp.021114.140715a Published online by Cambridge University Press

In summary, the truncation error of our adaptive finite element method with hybrid basis is uniformly convergent to zero for all $\varepsilon > 0$. It is easy to see that our schemes (A.15), (A.18), (A.22) satisfy the discrete maximum principle, then we have the following theorem:

Theorem A.1. *Our adaptive finite element method with hybrid basis schemes* (A.15), (A.18), (A.22) *have the following error estimate for the singularly perturbed two point boundary value problem* (A.1)-(A.2)*:*

$$\max_{0\le i\le N}|u_i-u(x_i)|\le\begin{cases}\frac{C}{N^2}+\frac{CN\varepsilon^2}{\varepsilon N\ln N+1}+C\varepsilon^2, & \varepsilon<\gamma,\\ \frac{C}{N^2\varepsilon^2}, & \varepsilon\ge\gamma,\end{cases} \tag{A.25}$$

where C is a constant independent of N and ε. Especially our AFEM-HB has the following minimum uniform convergence result for all $\varepsilon>0$:

$$\max_{0\le i\le N}|u_i-u(x_i)|\le\frac{C}{(N\ln N)^{\frac{2}{3}}}. \tag{A.26}$$

At last, we also note that for our adaptive finite element method with hybrid basis, the convergence order changes with ε. Our method has the minimum convergence order $\frac{2}{3}$ only when ε meets its transition point γ. It will converge faster if ε is away from γ. For example, when ε is $\mathcal{O}(1)$, the convergence result will be $\mathcal{O}(1/N^2)$; and when $\varepsilon<1/N$ is sufficiently small, then the convergence result will be $\mathcal{O}(1/N^2+\varepsilon/\ln N)$. These have been numerically verified in the previous Section 4.

Acknowledgments

This work was done when the author was visiting the Department of Mathematics at National University of Singapore, under the financial support of China Scholarship Council. This work was also partially supported by the NSFC Projects No. 11322113, 91330203, the National Basic Research Program of China under the grant 2011CB309705. The author would like to thank Prof. Weizhu Bao and Prof. Zhongyi Huang for very helpful discussion on this work.

References

[1] S. K. Adhikari, Numerical solution of the two-dimensional Gross-Pitaevskii equation for trapped interacting atoms, Phys. Lett. A, 265 (2000), 91.
[2] A. Aftalion and Q. Du, Vortices in a rotating Bose-Einstein condensate: Critical angular velocities and energy diagrams in the Thomas-Fermi regime, Phys. Rev. A, 64 (2001), 063603.
[3] M. H. Anderson, J. R. Ensher, M. R.Matthewa, C. E. Wieman and E. A. Cornell, Observation of Bose-Einstein condensation in a dilute atomic vapor, Science, 269 (1995), 198–201.
[4] W. Bao, Ground states and dynamics of multi-component Bose-Einstein condensates, Multiscale Modeling and Simulation, 2 (2004), 210–236.

https://doi.org/10.4208/cicp.021114.140715a Published online by Cambridge University Press

[5] W. Bao and Y. Cai, Mathematical theory and numerical methods for Bose-Einstein condensation, Kinet. Relat. Mod., 6 (2013), 1–135.
[6] W. Bao, Y. Cai and H. Wang, Efficient numerical methods for computing ground states and dynamics of dipolar Bose-Einstein condensates, J. Comput. Phys., 229 (2010), 7874–7892.
[7] W. Bao, I-L. Chern and Y. Zhang, Efficient methods for computing ground states of spin-1 Bose-Einstein condensates based on their characterizations, J. Comput. Phys., 253 (2013), 189–208.
[8] W. Bao and M. H. Chai, A uniformly convergent numerical method for singularly perturbed nonlinear eigenvalue problem, Commun. Comput. Phys. 4 (2008), 135–160.
[9] W. Bao and Q. Du, Computing the ground state solution of Bose-Einstein condensates by a normalized gradient flow, SIAM J. Sci. Comput., 25 (2004), 1674–1697.
[10] W. Bao, I.-L. Chern and F. Y. Lim, Efficient and spectrally accurate numerical methods for computing ground and first excited states in Bose-Einstein condensates, J. Comput. Phys., 219 (2006), 836–854.
[11] W. Bao, D. Jaksch and P. A. Markowich, Numerical solution of the Gross-Pitaevskii equation for Bose-Einstein condensation, J. Comput. Phys., 187 (2003), 318–342.
[12] W. Bao and F. Y. Lim, Computing ground states of spin-1 Bose-Einstein Condensates by the normalized gradient flow, SIAM J. Sci. Comput., 34 (2008), 1985–2008.
[13] W. Bao, F. Y. Lim and Y. Zhang, Energy and chemical potential asymptotics for the ground state of Bose-Einstein condensates in the semiclassical regime, Bull. Inst. Math., Academia Sinica, 2 (2007), 495–532.
[14] W. Bao and W. Tang, Ground state solution of trapped interacting Bose-Einstein condensate by directly minimizing the energy functional, J. Comput. Phys., 187 (2003), 230–254.
[15] W. Bao and H. Wang, A mass and magnetization conservative and energy diminishing numerical method for computing ground state of spin-1 Bose-Einstein condensates, SIAM J. Numer. Anal., 45 (2007), 2177–2200.
[16] W. Bao, H. Wang and P. A. Markowich, Ground, symmetric and central vortex states in rotating Bose-Einstein condensates, Commun. Math. Sci., 3 (2005), 57–88.
[17] H. Chen, L. He and A. Zhou, Finite element approximations of nonlinear eigenvalue problems in quantumn physics, Comput. Methods Appl. Mech. Engrg., 200 (2011), 1846–1865.
[18] P. G. Ciarlet, The Finite Element Method for Elliptic Problems, North-Holland, Amsterdam, 1978.
[19] M. M. Cerimele, M. L. Chiofalo, F. Pistella, S. Succi and M. P. Tosi, Numerical solution of the Gross-Pitaevskii equation using an explicit finite-difference scheme: An application to trapped Bose-Einstein condensates, Phys. Rev. E, 62, 1382 (2000).
[20] S.-M. Chang, W.-W. Lin and S.-F. Shieh, Gauss-Seidel-type methods for energy states of a multi-component Bose-Einstein condensate, J. Comput. Phys., 202 (2005), 367–390.
[21] R. C. Y. Chin and R. Krasny, A hybrid asymptotic finite element method for stiff two-point boundary value problems. SIAM J. Sci. Comput., 4 (1983), 229–243.
[22] M. L. Chiofalo, S. Succi and M. P. Tosi, Ground state of trapped interacting Bose-Einstein condensates by an explicit imaginary-time algorithm, Phys. Rev. E, 62 (2000), 7438.
[23] F. Dalfovo and S. Stringari, Bosons in anisotropic traps: Ground state and vortices, Phys. Rev. A, 53 (1996), 2477.
[24] X. Dai, J. Xu and A. Zhou, Convergence and optimal complexity of adaptive finite element eigenvalue computations, Numer. Math., 110 (2008), 313–355.
[25] R. J. Dodd, Approximate solutions of the nonlinear Schrödinger equation for ground and excited states of Bose-Einstein condensates, J. Res. Natl. Inst. Stan., 101 (1996), 545.

https://doi.org/10.4208/cicp.021114.140715a Published online by Cambridge University Press

[26] M. Edwards and K. Burnett, Numerical solution of the nonlinear Schrödinger equation for small samples of trapped neutral atoms, Phys. Rev. A, 51 (1995), 1382.
[27] H. Han and Z. Huang, Tailored finite point method for steady-state reaction-diffusion equation, Commun. Math. Sci., 8 (2010), 887–899.
[28] H. Han and Z. Huang, Tailored finite point method based on exponential bases for convection-diffusion-reaction equation, Math. Comp., 82 (2013), 213–226.
[29] H. Han and Z, Huang, The Tailored Finite Point Method, Comput. Methods Appl. Math. 14 (2014), 321–345.
[30] H. Han, Z. Huang and B. Kellogg, A Tailored finite point method for a singular perturbation problem on an unbounded domain, J. Sci. Comput., 36 (2008), 243–261.
[31] H. Han, J. J. H. Miller and M. Tang, A parameter-uniform tailored finite point method for singularly perturbed linear ODE systems, J. Comput. Math. 31 (2013), 422–438.
[32] L. Jiang and X. Yue, Local exponentially fitted fnite element schemes for singularly perturbed convection-diffusion problems, J. Comput. Appl. Math., 132 (2001), 277–293.
[33] R. Lin and M. Stynes, A balanced finite element method for singularly perturbed reaction diffusion problems, SIAM J. Numer. Anal., 50 (2012), 2729–2743.
[34] J. M. Melenk, hp-finite element methods for singular perturbations, Lecture Notes in Mathematics, 1796. Springer-Verlag, Berlin, 2002.
[35] J. J. H. Miller, E. ORiordan and G. I. Shishkin, Fitted Numerical Mehtods for Sigular Perturbation Problems, World Scientific, 1996.
[36] J. J. H. Miller, E. ORiordan and G. I. Shishkin, On piecewise-uniform meshes for upwindand central-difference operators for solving singularly perturbed problems, IMA J. Numer. Anal., 15 (1995), 89–99.
[37] L. P. Pitaevskii and S. Stringari, Bose-Einstein Condensation, Clarendon Press, 2003.
[38] E. O'Riordan, M. Stynes, A uniformly accurate finite-element method for a singularly perturbed one dimensional reaction-diffusion problem, Math. Comp., 47 (1986), 555–570.
[39] H. G. Roos, M. Stynes and L. Tobiska, Numerical Methods for Singularly Perturbed Differential Equations, Springer-Verlag, Berlin, 2nd ed., 2008.
[40] B. I. Schneider and D. L. Feder, Numerical approach to the ground and excited states of a Bose-Einstein condensated gas confined in a completely anisotropic trap, Phys. Rev. A, 59 (1999), 2232.
[41] L. Shen, J. Xin and A. Zhou, Finite element computation of KPP front speeds in celluar and cats eye flows, J. Sci. comput., 55 (2013), 455–470.
[42] L. Shen and A. Zhou, A defect correction scheme for finite element eigenvalues with applications to quantum chemistry, SIAM J. Sci. Comput., 28 (2006), 321–338.
[43] M. Stynes, E. ORiordan, An analysis of a singularly perturbed two-point boundary problem using only finite element techniques, Math. Comp., 56 (1991), 663–675.
[44] Y. Qiu, D. M. Sloan and T. Tang, Numerical solution of a singularly perturbed two-point boundary value problem using equidistribution: analysis of convergence, J. Comput. Appl. Math., 116 (2000), 121–143.
[45] A. Zhou, Finite dimensional approximations for the electronic ground state solution of a molecular system, Math. Methods Appl. Sci., 30 (2007), 429–447.
[46] A. Zhou, An analysis of finite-dimensional approximations for the ground state solution of Bose-Einstein condensates, Nonlinearity, 17 (2004), 541–550.

https://doi.org/10.4208/cicp.021114.140715a Published online by Cambridge University Press